Title

Autophagy restricts Mycobacterium tuberculosis during acute infection in mice

Journal

Nature Microbiology, 8(5)

ISSN

2058-5276

Authors

Golovkine, Guillaume R

Roberts, Allison W

Morrison, Huntly M

et al.

Publication Date

2023-05-01

DOI

10.1038/s41564-023-01354-6

Peer reviewed

HHS Public Access

Author manuscript

Nat Microbiol. Author manuscript; available in PMC 2024 April 19.

Published in final edited form as:

Nat Microbiol. 2023 May ; 8(5): 819–832. doi:10.1038/s41564-023-01354-6.

Autophagy restricts *Mycobacterium tuberculosis* during acute infection in mice

Guillaume R. Golovkine[1,7], **Allison W. Roberts**[1], **Huntly M. Morrison**[1], **Rafael Rivera-Lugo**[1], **Rita M. McCall**[2], **Hannah Nilsson**[1], **Nicholas E. Garelis**[1], **Teresa Repasy**[1,8], **Michael Cronce**[3,4], **Jonathan Budzik**[1,5,9], **Erik Van Dis**[1,10], **Lauren M. Popov**[1,11], **Gabriel Mitchell**[1,12], **Reena Zalpuri**[6], **Danielle Jorgens**[6], **Jeffery S. Cox**[1,✉]

[1]Department of Molecular and Cell Biology, University of California, Berkeley, CA, USA.

[2]Department of Plant & Microbial Biology, University of California, Berkeley, CA, USA.

[3]Department of Bioengineering, University of California, Berkeley, CA, USA.

[4]UC Berkeley—UCSF Graduate program in Bioengineering, Berkeley, CA, USA.

[5]Department of Medicine, University of California, San Francisco, CA, USA.

[6]Electron Microscope Laboratory, University of California, Berkeley, CA, USA.

[7]Present address: Evotec, Toulouse, France.

[8]Present address: Bio-Rad Laboratories, Seattle, WA, USA.

[9]Present address: Department of Medicine, University of California, San Francisco, CA, USA.

[10]Present address: Department of Immunology, University of Washington School of Medicine, Seattle, WA, USA.

[11]Present address: Novome Biotechnologies, San Francisco, CA, USA.

[12]Present address: Open Innovation @ NITD, Novartis Institute for Tropical Diseases, Emeryville, CA, USA.

✉ **Correspondence and requests for materials** should be addressed to Jeffery S. Cox. jeff.cox@berkeley.edu.

Author contributions

J.S.C., G.R.G. and G.M. conceptualized the study. G.R.G. was responsible for conducting experiments, acquisition of data and analysis. G.R.G. and M.C. performed qPCR experiments. N.G. performed RNA-seq data analysis. G.R.G. and L.M.P. performed live imaging experiments. L.M.P., G.M. and J.S.C. provided reagents. G.R.G., A.W.R., R.M.M., H.M., T.R., J.B. and E.V.D. performed in vivo experiments. G.R.G., R.R.-L. and R.M.M. performed *M. marinum* experiments. G.R.G. and H.M. performed immunofluorescence experiments. G.R.G., D.J. and R.Z. conducted electron microscopy experiments. G.R.G. and H.N. performed western blot experiments. G.R.G. and J.S.C. wrote the paper.

Competing interests

The authors declare no competing interests.

Reporting summary

Further information on research design is available in the Nature Portfolio Reporting Summary linked to this article.

Additional information

Extended data is available for this paper at https://doi.org/10.1038/s41564-023-01354-6.

Supplementary information The online version contains supplementary material available at https://doi.org/10.1038/s41564-023-01354-6.

Peer review information *Nature Microbiology* thanks Maziar Divangahi, Vojo Deretic and the other, anonymous, reviewer(s) for their contribution to the peer review of this work.

Abstract

Whether or not autophagy has a role in defence against *Mycobacterium tuberculosis* infection remains unresolved. Previously, conditional knockdown of the core autophagy component ATG5 in myeloid cells was reported to confer extreme susceptibility to *M. tuberculosis* in mice, whereas depletion of other autophagy factors had no effect on infection. We show that doubling *cre* gene dosage to more robustly deplete ATG16L1 or ATG7 resulted in increased *M. tuberculosis* growth and host susceptibility in mice, although ATG5-depleted mice are more sensitive than ATG16L1- or ATG7-depleted mice. We imaged individual macrophages infected with *M. tuberculosis* and identified a shift from apoptosis to rapid necrosis in autophagy-depleted cells. This effect was dependent on phagosome permeabilization by *M. tuberculosis*. We monitored infected cells by electron microscopy, showing that autophagy protects the host macrophage by partially reducing mycobacterial access to the cytosol. We conclude that autophagy has an important role in defence against *M. tuberculosis* in mammals.

Macro-autophagy (hereafter termed ‘autophagy’) encapsulates large intracellular cargos in a double-membrane structure named the autophagosome[1,2]. Upon fusion of the autophagosome with a lysosome, the cargo is degraded by lysosomal proteases[3]. Autophagy has pleiotropic roles in eukaryotic cellular homoeostasis. While different cellular components are targeted to autophagy machinery in response to various cellular stresses, autophagy of intracellular pathogens (xenophagy) has an evolutionarily conserved and fundamental role in host defence against infection[2,3]. Delivery of intracellular pathogens to lysosomes limits pathogen replication. Autophagy also mediates disease progression by regulating inflammatory signalling in response to infection[4–6] but the mechanism by which this occurs is not completely understood.

Autophagy cargo, including intracellular pathogens, are targeted by a range of receptors[2], through modification with ubiquitin or other proteins such as Galectin-3, -8 and -9, which recognize damaged membranes[7,8]. Canonical autophagy starts with the formation of a prophagophore via the fusion of FIP200- and ATG16L1-positive vesicles[2]. Two ubiquitin-like enzymatic cascades, including ATG7, ATG3 and a complex of ATG12–ATG5 and ATG16L1 function to lipidate the autophagy factor LC3-I (a member of the ATG8 family of proteins) to form LC3-II, which in turn localizes to the phagophore and participates in a membrane stress and remodelling response[2,3]. These proteins are often referred to as part of the core autophagy machinery, although in some cases LC3 lipidation can be bypassed[2,3].

Mycobacterium tuberculosis is an intracellular pathogen of humans that replicates in macrophages and thrives under inflammatory states in vivo[9–11]. Although autophagy targets and restricts *M. tuberculosis* growth in cultured macrophages[12], the importance of autophagy in resistance to *M. tuberculosis* infection in whole animal models of infection has been controversial[13,14]. Core autophagy components are essential for mouse development[2].

Early experiments using a ‘floxed’ *Atg5* allele (*Atg5*$^{fl/fl}$) in combination with a single copy of the *LysMcre* expression construct (*LysMcre*$^{+/-}$) to specifically delete *Atg* genes from myeloid cells, showed that autophagy restricts mycobacterial replication in primary cultured macrophages[15] and that these mice are extremely susceptible to *M. tuberculosis*

infection and have a heightened pro-inflammatory state. The conclusion at that time was that autophagy is an important part of the host response to *M. tuberculosis*[15,16]. Subsequent work by ref. 13 showed that depletion of core autophagy genes other than *Atg5* did not result in susceptibility of mice to *M. tuberculosis* during the first 12 weeks of infection. This led them to propose that ATG5 has a non-autophagy role in host defence against *M. tuberculosis* and that autophagy is not, per se, a important mechanism of defence in the murine model of infection[13,14]. The broader implication was a re-evaluation of the value of harnessing the autophagy pathway as a potential target for host-directed therapeutics and vaccine design to fight tuberculosis[17].

Here, we further investigate the role of autophagy during infection of mice with *M. tuberculosis*. We use the same genetically modified mouse lines as those used in ref. 13 to investigate how varying Cre-mediated recombination efficiency between different floxed *Atg* genes affects autophagy inhibition and *M. tuberculosis* infection outcomes and report our results here.

Results

Efficiency of deletion of different autophagy genes using Cre–Lox

To test if differences in recombination efficiency of individual floxed *Atg* alleles correlated with the observed infection phenotypes, we measured Cre-mediated recombination of three different core autophagy genes—*Atg5*, *7* and *16L1*—by semiquantitative PCR in bone marrow-derived macrophages (BMMs) isolated from these mice. The mice contained one copy of the Cre recombinase gene expressed from the *Lyz2* locus (*LysMcre*$^{+/-}$) to conditionally inhibit expression in myeloid cells, including macrophages[18]. We isolated haematopoetic precursor cells from bone marrow of *Atg5*$^{fl/fl}$ *LysMcre*$^{+/-}$, *Atg16L1*$^{fl/fl}$ *LysMcre*$^{+/-}$ and *Atg7*$^{fl/fl}$ *LysMcre*$^{+/-}$ mice, differentiated them into BMMs by culturing in the presence of CSF-1 and collected genomic DNA after 7, 10 and 12 days of differentiation. We used semiquantitative PCR to amplify junctions of the non-recombined and recombined genomic loci for each of the three mouse genes and calculated the percentage recombination in the bulk cell population (Fig. 1). Cre-mediated recombination was very efficient (81%) in *Atg5*$^{fl/fl}$ *LysMcre*$^{+/-}$ BMMs after 7 days of differentiation and the percentage recombination increased further over time (Fig. 1a, lanes 1–6). However, the recombination efficiency observed in *Atg16L1*$^{fl/fl}$ *LysMcre*$^{+/-}$ (Fig. 1b, lanes 1–6) and *Atg7*$^{fl/fl}$ *LysMcre*$^{+/-}$ (Fig. 1c, lanes 1–6) BMMs was lower than for *Atg5*$^{fl/fl}$ *LysMcre*$^{+/-}$ (55% and 75%, respectively, at day 7). In both cases, there was no increase in recombination during the extended time in culture (Fig. 1b,c, lanes 4–6). The *Atg16L1*$^{fl/fl}$ allele appears to be particularly resistant to Cre-mediated recombination, as we achieved a maximum of only 60% recombination. Thus, in primary macrophages isolated from mice with only one copy of *LysMcre*, the *Atg7* and *Atg16L1* alleles are hypomorphic.

Efficiency of *cre–lox* recombination can be affected by several factors, including the length of the intervening DNA between the two *loxP* sites[19], accessibility of Cre recombinase to the *loxP* sites within different genomic contexts[19], levels of Cre expression[20] and mutations in the *loxP* sites[21]. PCR amplification and sequencing of the six *loxP* sites that flank the three genomic recombination substrates confirmed that each had identical, wild-type

sequences and thus had not accumulated mutations that would interfere with Cre recognition (Extended Data Fig. 1a). The size of the intervening sequence between the pairs of *loxP* sites are 2,260 base pairs (bp), 729 bp and 2,539 bp for $Atg5^{fl/fl}$, $Atg16L1^{fl/fl}$ and $Atg7^{fl/fl}$, respectively (Extended Data Fig. 1b). The *LysMcre* expression constructs are identical between all three mouse strains and quantitative PCR with reverse transcription (qRT–PCR) analysis indicated that *cre* messenger RNA levels were similar between the three mutants (Extended Data Fig. 1c). Thus, we have ruled out sequence or expression differences that would explain the differences in recombination efficiency between the three floxed *Atg* genes, making it likely that the unique genomic context at each locus limits access of Cre to its substrate.

Increasing *LysMcre* dosage to decrease autophagy gene expression

We reasoned that increasing Cre expression may promote catalysis and drive greater reduction in gene expression of *Atg16L1* and *Atg7*. To this end, we crossed the mice described above to yield strains that were identical except that they were homozygous at the *Lyz2* locus ($LysMcre^{+/+}$) and thus would be expected to express greater levels of Cre recombinase via gene dosage. Importantly, the additional copy of *LysMcre* led to increased efficiency of recombination of both $Atg16L1^{fl/fl}$ and $Atg7^{fl/fl}$ in BMMs compared to cells isolated from hemizygous *LysMcre* mice (Fig. 1b and c, lanes 4–9). While recombination at the *Atg7* locus was nearly complete in these cells, some unrecombined *Atg16L1* was still present at detectable levels. Although *cre–lox* recombination was already very efficient in $Atg5^{fl/fl}$ $LysMcre^{+/-}$ BMMs, it was further enhanced in $Atg5^{fl/fl}$ $LysMcre^{+/+}$ (Fig. 1a, lanes 4–9). Thus, for each of these three *Atg* genes, we constructed mouse strains homozygous for the respective floxed allele that encode either zero ($LysM^{wt/wt}$), one (hemizygous) or two (homozygous) copies of *LysMcre* to create a gene-dosage series of Cre that varied in level of recombination efficiency.

Functional effects of *LysMcre* dosage on *Atg* gene expression

To test the functional consequence of increased DNA recombination on *Atg* gene expression, we performed qRT–PCR using RNA collected from BMMs derived from these mice after 10 days of differentiation. In hemizygous *LysMcre* cells, mRNA levels of the genes were significantly reduced compared to $LysM^{wt/wt}$ controls but showed higher residual expression of both *Atg16L1* (27% remaining) and *Atg7* (16%) compared to *Atg5* (9%), mirroring the relative differences in DNA recombination efficiency (Fig. 1d–f). Importantly, doubling *LysMcre* copy number led to a concomitant further decrease in *Atg* mRNA levels (Fig. 1d–f). The mRNA levels for *Atg5*, *Atg16L1* and *Atg7* were 0.8%, 2.7% and 1.8%, respectively. We also measured autophagy activity in these cells by quantifying conversion of LC3 from its precursor form (LC3-I) to its activated, cleaved form (LC3-II) by western blotting. In unstimulated BMMs, we observed equivalent LC3 conversion in $LysM^{wt/wt}$ control macrophages for all three *Atg* genotypes, indicative of baseline autophagic flux (Fig. 1g, lanes 1, 4 and 7). The LC3-II:LC3-I ratio was reduced in all three of the hemizygous *LysMcre* cells, indicating decreased autophagic flux under homoeostatic conditions where the steady-state ratio of LC3-I and LC3-II is governed by both cleavage of LC3-I and lysosomal degradation of LC3-II (Fig. 1g). We detected an even greater reduction in this ratio in the *cre*-homozygous macrophages, although differences between the various

Atg genes were not apparent under these conditions. To more sensitively detect differences in the ability of these cells to activate autophagy, we stimulated the pathway (and thus LC3-I to LC3-II cleavage) by incubating for 8 h in nutrient-deficient media and stabilizing LC3-II inside cells by blocking autophagic flux with the addition of bafilomycin over the last 2 h before collecting proteins for western blotting (Fig. 1h, +EBSS +bafilomycin)[22]. Conversion of LC3-I to LC3-II was strongly blocked in $Atg5^{fl/fl}$ $LysMcre^{+/-}$ cells. In contrast, we observed only partial blockage of autophagy in $Atg16L1^{fl/fl}$ $LysMcre^{+/-}$ (LC3-II:LC3-I ratio = 0.66). The autophagy blockage in $Atg7^{fl/fl}$ $LysMcre^{+/-}$ (0.34) cells was close to that observed in $Atg5^{fl/fl}$ $LysMcre^{+/-}$ (0.31, Fig. 1h). In all cases, an additional copy of *cre* led to further reduction in LC3 cleavage. These results are consistent with the reduced efficiency of Cre-mediated recombination in these cells (Fig. 1a–c) and indicate that while one copy of *LysMcre* is sufficient to fully inhibit ATG5 activity, the floxed A$tg16L1^{fl/fl}$, and to a lesser extend $Atg7^{fl/fl}$, are hypomorphic under these conditions.

Atg7 and *Atg16L1* deletion renders mice susceptible to *M. tuberculosis*

Because of the hypomorphic nature of the *Atg7* and *Atg16L1* conditional alleles in cells isolated from hemizygous *LysMcre* mice, it is plausible that the residual autophagy activity in these mice is sufficient to provide resistance to *M. tuberculosis* infection. Increasing recombination efficiency may then inhibit autophagy beyond a critical threshold for resistance to infection. Thus, we performed low-dose aerosol infections with virulent *M. tuberculosis* (Erdman) in the three floxed *Atg* mice carrying zero, one and two copies of *LysMcre* and evaluated them for weight loss and survival. As previously observed[13,15,16], $Atg5^{fl/fl}$ $LysMcre^{+/-}$ mice succumbed rapidly to *M. tuberculosis* infection, marked by a precipitous drop in weight loss during the acute stage of infection (Fig. 2a and Extended Data Fig. 3a). These mice were killed after 2–3 weeks when they lost 15% of their starting weight (Fig. 2d). We observed no further increase in susceptibility in the $Atg5^{fl/fl}$ $LysMcre^{+/+}$ mice (Fig. 2a,d and Extended Data Fig. 3a). Surprisingly, we found that $Atg16L1^{fl/fl}$ $LysMcre^{+/-}$ mice were more susceptible to *M. tuberculosis* than $Atg16L1^{fl/fl}$ mice, as they lost weight during the acute phase (Fig. 2b and Extended Data Fig. 3b) and eventually succumbed faster than the $Atg16L1^{fl/fl}$ control during the chronic stages of infection (Fig. 2e). This phenotype was not identified by ref. 13 as they focused their analysis on the first 12 weeks postinfection[13]. Importantly, increased homozygous *LysMcre* expression further decreased resistance to *M. tuberculosis* in these mice, leading to a sharp drop in weight (−10%) during acute infection and accelerated mortality (Fig. 2b,e and Extended Data Fig. 3b). While the $Atg5^{fl/fl}$ $LysMcre^{+/+}$ mice were more sensitive than $Atg16L1^{fl/fl}$ $LysMcre^{+/+}$ mice, the sharp decline in weight loss in $Atg16L1^{fl/fl}$ $LysMcre^{+/+}$ mice is notable and similar to infected $Atg5^{fl/fl}$ $LysMcre^{+/-}$ mice in the first 3 weeks of infection. The $Atg7^{fl/fl}$ $LysMcre^{+/-}$ mice were not significantly more susceptible than the $Atg7^{fl/fl}$ control although their weight gain was stunted during the first 12 weeks of infection but $Atg7^{fl/fl}$ $LysMcre^{+/+}$ mice were significantly more sensitive to infection than the control (Fig. 2c,f and Extended Data Fig. 3c). Whether the difference between *Atg5* and the other autophagy genes is due to a unique role of ATG5 or an increased depletion of the protein remains an open question, however, it is clear that by further decreasing ATG7 and ATG16L1 levels, we have found that these core autophagy factors are also important for *M. tuberculosis* control.

Autophagy restricts *M. tuberculosis* during acute infection

We also collected organs to evaluate bacterial burden and lung lesions at days 21 and 70 postinfection. As expected from previous results[13,15], we observed increased bacterial burden in the lungs of *Atg5*$^{fl/fl}$ *LysMcre*$^{+/-}$ and *Atg5*$^{fl/fl}$ *LysMcre*$^{+/+}$ mice compared to the *Atg5*$^{fl/fl}$ controls at 21 days postinfection (25-fold increase, Fig. 3a), associated with extensive lung lesions (Fig. 3c,e). In contrast, there was no difference in colony-forming units (c.f.u.) (Fig. 3a) or size of lesions (Fig. 3c) in the lungs of *Atg16L1*$^{fl/fl}$ *LysMcre*$^{+/-}$ and *Atg7*$^{fl/fl}$ *LysMcre*$^{+/-}$ mice compared to their respective flox controls. However, we observed a significant increase in c.f.u. in *Atg16L1*$^{fl/fl}$ *LysMcre*$^{+/+}$ and *Atg7*$^{fl/fl}$ *LysMcre*$^{+/+}$ mice (tenfold and sixfold, respectively, Fig. 3a), mirroring the increase in *cre*-mediated recombination described in Fig. 1. Thus, autophagy is important for controlling bacterial growth during the acute phase of infection.

Interestingly, 70 days after infection, c.f.u. levels in *Atg16L1*$^{fl/fl}$ *LysMcre*$^{+/+}$ and *Atg7*$^{fl/fl}$ *LysMcre*$^{+/+}$ mice had receded to levels similar to the respective flox controls (Fig. 3b), demonstrating that autophagy-mutant mice manage to control *M. tuberculosis* growth in the chronic phase of the infection, probably due to the onset of adaptive immunity. Despite nearly equivalent levels of bacteria at this time point, inflammatory lesions were larger and more pronounced in the lungs of *Atg16L1*$^{fl/fl}$ *LysMcre*$^{+/+}$ and *Atg7*$^{fl/fl}$ *LysMcre*$^{+/+}$ mice (Fig. 3d,f). The differences in bacterial burdens we observed in lungs were not recapitulated in the spleens and the bacterial numbers remained constant throughout infection (Extended Data Fig. 3d,e).

Autophagy depletion promotes neutrophil influx in lungs during acute infection

To evaluate the cellular inflammatory responses to infection, we used flow cytometry to quantify relative proportions of immune cells from the lungs of autophagy-mutant mice infected with *M. tuberculosis* for 21 and 70 days (Extended Data Fig. 2). As described previously[13], significantly more neutrophils were recruited in the lungs of *Atg5*$^{fl/fl}$ *LysMcre*$^{+/-}$ mice compared to *Atg5*$^{fl/fl}$ mice at 21 days postinfection and similar to *Atg5*$^{fl/fl}$ *LysMcre*$^{+/+}$ mice (Fig. 2g). We also observed high levels of neutrophil influx in the lungs of *Atg16L1*$^{fl/fl}$ *LysMcre*$^{+/-}$ and *Atg7*$^{fl/fl}$ *LysMcre*$^{+/-}$ mice at day 21 postinfection (Fig. 2h, i) and the proportion of neutrophils was further increased in *cre*-homozygous mice (Fig. 2h,i). At day 70 after infection, despite equivalent bacteria burdens in the lungs (Fig. 3b), the proportion of neutrophils remained higher in *Atg16L1*$^{fl/fl}$ *LysMcre*$^{+/+}$ and *Atg7*$^{fl/fl}$ *LysMcre*$^{+/+}$ mice (Extended Data Fig. 3f,g), mirroring the persistent increase in chronic inflammatory lesions in the tissue. The percentage of T cells at 70 days postinfection was higher than at 21 days, indicative of specific immune responses and the levels were unaffected by autophagy depletion. Taken together, the decreased lifespan of infected *Atg16L1*$^{fl/fl}$ *LysMcre*$^{+/+}$ and *Atg7*$^{fl/fl}$ *LysMcre*$^{+/+}$ mice was probably due to greater pulmonary inflammatory disease marked by high numbers of neutrophils during the chronic phase of infection, consistent with the growing literature of the negative effects of neutrophils on resistance to *M. tuberculosis* infection[23,24].

Lysozyme 2 does not contribute to susceptibility in autophagy-deficient mice

Since the *cre* gene replaces the *Lys2* open reading frame in the *LysMcre* locus, the increased susceptibility of *Atg16L1*$^{fl/fl}$ *LysMcre*$^{+/+}$ and *Atg7*$^{fl/fl}$ *LysMcre*$^{+/+}$ mice could be due to deficiency in lysozyme 2. However, infection of *LysMcre*$^{+/+}$ mice gave rise to wild-type levels of susceptibility (Fig. 2c,f and Extended Data Fig. 3c), bacterial burdens (Fig. 3a,b and Extended Data Fig. 3d,e), lung pathology (Fig. 3c,d) and composition of cellular infiltrates (Fig. 2i and Extended Data Fig. 3g) as *Atg*$^{fl/fl}$ control mice. These results demonstrate that lysozyme 2 deficiency does not alter resistance to *M. tuberculosis* and rule out potential effects of Cre-mediated toxicity reported for other mouse models[25,26].

Autophagy-deficient macrophages are sensitive to *M. tuberculosis*

We noted previously that *M. tuberculosis* infection of *Atg5*$^{fl/fl}$ *LysMcre*$^{+/-}$ BMMs led to increased bacterial growth[15] but we were unable to carry infections out for longer than 48 h due to disruptions in monolayer integrity, suggesting that autophagy controls cell death. Because the mode of macrophage cell death has a profound impact on inflammatory responses and *M. tuberculosis* pathogenesis[27], we sought to directly assess the role of autophagy in macrophage viability during infection. To this end, we performed live, time-lapse light microscopy imaging of *Atg5fl/fl*, *Atg5fl/fl LysMcre+/+*, *Atg16L1fl/fl*, *Atg16L1fl/fl LysMcre+/+*, *Atg7fl/fl* and *Atg7*$^{fl/fl}$ *LysMcre*$^{+/+}$ BMMs infected with GFP-expressing *M. tuberculosis*. Macrophage viability was assessed by monitoring morphological features of cell death including cessation of movement, cell rounding and change in refractive index. *Atg5*$^{fl/fl}$ *LysMcre*$^{+/+}$ macrophages were extremely susceptible to *M. tuberculosis* (Fig. 4a and Supplementary Video 1) and rounding and death of most cells appeared between days 2 and 3 of infection. *Atg7*$^{fl/fl}$ *LysMcre*$^{+/+}$ BMMs were almost as susceptible, with rounded cells starting to appear 3 days after infection (Fig. 4a), while the onset of cell death in *Atg16L1*$^{fl/fl}$ *LysMcre*$^{+/+}$ cells was delayed by ~2 days (Fig. 4a). By 6 days postinfection, all three autophagy-deficient macrophage monolayers were severely disrupted whereas control monolayers remained mostly intact. Using high-content microscopy, quantification of cell numbers over time mirrored the results of the live imaging experiment (Fig. 4b and statistics in Extended Data Fig. 4a). All *LysMcre*-homozygous macrophages were more susceptible than their *LysMcre*-hemizygous counterparts (Fig. 4b), an effect that was independent of Lysozyme 2 deficiency (Extended Data Fig. 5b).

Quantification of intracellular bacterial growth over time, estimated by measuring mean fluorescent intensity of GFP-*M. tuberculosis* by high-content microscopy, revealed that both *Atg5*$^{fl/fl}$ *LysMcre*$^{+/-}$ and *Atg5*$^{fl/fl}$ *LysMcre*$^{+/+}$ were significantly more permissive for bacterial growth than control cells (Fig. 4c and statistics in Extended Data Fig. 4b). *Atg16L1*$^{fl/fl}$ *LysMcre*$^{+/-}$ and *Atg7*$^{fl/fl}$ *LysMcre*$^{+/-}$ BMMs had an intermediate effect on bacterial growth and homozygous *LysMcre* cells led to equivalent growth rates as in *Atg5*-deficient cells. This data were confirmed by c.f.u. plating (Extended Data Fig. 5a). In the time-lapse videos, we also observed increased fluorescence after macrophage death, consistent with other work reporting *M. tuberculosis* growth inside necrotic macrophages[28,29], an effect that was much more pronounced in autophagy-depleted cells (Fig. 4a and Supplementary Video 1). Altogether, these data demonstrate that core autophagy components restrict bacterial growth and prevent macrophage death.

Autophagy counters cell death by inhibiting phagosome escape

Recent work linking autophagy and membrane repair[30,31] suggested that autophagy may antagonize phagosomal permeabilization mediated by the ESX-1 Type VII secretion system of *M. tuberculosis*[15,32–34]. By limiting cytosolic access, autophagy may restrain activation of intracellular cell death pathways. We initially sought to test this idea by visualizing cellular membranes using uranyl acetate staining and transmission electron microscopy (TEM; Extended Data Fig. 6a,b). Although it is difficult to assess small membrane disruptions using TEM, we quantified the number of bacteria that were primarily bounded by host membranes and those that were not at 24 h postinfection. We found that the percentage of bacteria identified outside of phagosomes increased in autophagy-deficient macrophages (Extended Data Fig. 6b), although this assay requires exquisite membrane preservation and can be prone to artifacts. To independently assess mycobacterial phagosome escape, we used a closely related mycobacterial pathogen, *Mycobacterium marinum* that also uses ESX-1 to permeabilize the phagosome but unlike *M. tuberculosis* patently enters the cytosol and polymerizes actin tails[35,36]. Using phalloidin staining of actin tails in infected cells provides a robust and quantitative method to indirectly assess phagosome membrane integrity. While ~15% of intracellular *M. marinum* colocalized with actin tails in autophagy-competent cells 11 h after infection, we found that more intracellular *M. marinum* (~40–55%) polymerized actin tails in autophagy-deficient macrophages (Fig. 5a,b), indicating that autophagy functions to limit cytosolic access. Importantly, kinetics of formation of individual actin tails was equal between autophagy-deficient cells and control cells, indicating that the increased number of tails was due to decreased phagosome integrity (Extended Data Fig. 6c). We also used immunofluorescence microscopy to evaluate recruitment of galectin-3 to *M. tuberculosis*, which colocalizes to *M. tuberculosis* in response to phagosome permeabilization[37] (Extended Data Fig. 6d). We observed increased Gal-3 recruitment to *M. tuberculosis* in $Atg5^{fl/fl}$ $LysMcre^{+/-}$, $Atg16L1^{fl/fl}$ $LysMcre^{+/-}$ and $Atg7^{fl/fl}$ $LysMcre^{+/-}$ macrophages compared to controls. Galectin-3–*M. tuberculosis* colocalization was further increased in cell populations harbouring two copies of *LysMcre* (Extended Data Fig. 6d). Taken together, our results show that autophagy functions to limit ESX-1-mediated phagosome disruption and cytosolic access.

To investigate whether autophagy-dependent phagosome integrity during *M. tuberculosis* infection was responsible for increased cell death, we infected cells with a Δ*eccC* mutant strain lacking a central component of ESX-1 (ref. 38), which fails to permeabilize the phagosome and activate cytosolic sensors, yet still activates surface/phagosomal Toll-like receptor signalling[15,34,39–41]. Importantly, this strain failed to induce rapid cell death in any of the autophagy-mutant macrophages and failed to disrupt the monolayers over an extended period of time (Fig. 5c and Extended Data Fig. 7c), although it did promote slightly accelerated cell death when compared to uninfected cells (Extended Data Fig. 7a,b). Although an autophagy-dependent phenotype was apparent at very late stages of infection (>14 days), there was no sign of the extreme susceptibility observed with wild-type *M. tuberculosis*. These data indicate that ESX-1-mediated cytosolic access triggers the rapid necrotic cell death phenotype in autophagy-depleted macrophages.

Expression analysis of autophagy-deficient macrophages

To identify cellular pathways altered in autophagy-deficient cells, we performed RNA-seq on RNA collected from *Atg5*$^{fl/fl}$ *LysMcre*$^{+/+}$, *Atg16L1*$^{fl/fl}$ *LysMcre*$^{+/+}$ and *Atg7*$^{fl/fl}$ *LysMcre*$^{+/+}$ BMMs and their respective *LysM*$^{wt/wt}$ control cells, both after 48 h of infection with *M. tuberculosis* and mock-infection controls (Extended Data Fig. 8a–c). For uninfected *Atg16L1*- and *Atg7*-deficient macrophages, there were relatively few significantly differentially expressed genes (38 and 60, respectively) compared to unfloxed control cells (Extended Data Fig. 8d). In contrast, 377 genes were differentially expressed between uninfected *Atg5*-deficient cells and control cells, indicating that these cells responded differently to depletion than the *Atg16L1* and *Atg7* cells.

Upon infection, we identified 762, 235 and 390 differentially expressed genes for ATG5, ATG16L1 and ATG7, respectively. Comparison of the differentially expressed genes for all three genotypes identified 112 genes (11%) that were commonly regulated between them (Extended Data Fig. 8e). Interestingly, gene ontology pathway enrichment analysis on this gene set identified a significant enrichment for pathways involved in oxidative stress response and glutathione metabolism (Extended Data Fig. 8g), suggesting that ATG-deficient cells experience increased levels of oxidative stress. However, these pathways were no longer identified when we subtracted genes that were also differentially expressed in uninfected conditions (Extended Data Fig. 8d,f,h). Therefore, these oxidative stress pathways are independent of infection. Similar analysis on the ATG5-specific gene set did not identify a significant pathway enrichment (Extended Data Fig. 8i).

Surprisingly, we identified *Atg5* mRNA sequences in *Atg5*$^{fl/fl}$ *LysMcre*$^{+/+}$ macrophages, consistent with previous work showing that deletion of exon 3 resulted in the production of an incomplete mRNA lacking exon 3 (ref. 42). Infection of heterozygous *Atg5*$^{fl/wt}$ *LysMcre*$^{+/+}$ mice showed that the presence of this truncated mRNA does not exert a dominant effect on susceptibility (Extended Data Fig. 5b).

Autophagy promotes apoptosis of infected macrophages

Since pyroptosis has been implicated in *M. tuberculosis*-mediated cell death and is activated by cytosolic signals[43,44], we measured IL1β levels in supernatants of macrophages infected for 48 h with wild-type *M. tuberculosis* or Δ*eccC M. tuberculosis*. Wild-type *M. tuberculosis* induced secretion of IL1β, as previously described[45]. We detected higher levels in *Atg5*- and *Atg7*-deficient macrophages (both hemizygous and homozygous *cre*) compared to their respective *LysM*$^{wt/wt}$ controls (Extended Data Fig. 9b). However, there was no significant increase in IL1β in *Atg16L1*-depleted macrophages. The differences observed with *Atg5*- and *Atg7*-depleted cells were moderate and did not correlate with Cre expression, which suggests that pyroptosis is unlikely to be the primary mode of cell death in the absence of autophagy. ATG5 has also been previously linked with induction of apoptosis via Bcl-xL activation[46] and Bcl-xL also mediates RIPK3-dependent necrosis in macrophages infected with *M. tuberculosis*[47]. We assessed the levels of pRIP3 and Bcl-xL in *Atg5*, *Atg16L1* and *Atg7*-deficient macrophages and did not observe differences in expression compared to *LysM*$^{wt/wt}$ control cells (Extended Data Fig. 9a).

To visually assess necrosis and apoptotic cell death, we performed live imaging on infected macrophages incubated with propidium iodide (PI) and CellEvent Caspase-3/7 reagent, which stain cells undergoing necrosis and apoptosis, respectively. Importantly, the autophagy-deficient cells robustly incorporated PI when they died, indicating plasma membrane rupture with hallmarks of necrotic cell death (Fig. 6a, Extended Data Fig. 10a,c and Supplementary Video 2). The kinetics of PI staining with the *Atg16L1* mutant cells was slower than for *Atg5* and *Atg7*, consistent with our previous imaging of the timing of cell death (Fig. 3a). We detected only minimal fluorescence signal from the CellEvent probe in autophagy-deficient cells, indicating that the apoptosis pathway is not activated (Fig. 6b, Extended data Fig. 10a,b and Supplementary Video 2). Interestingly, after all the autophagy-deficient cells died in a necrotic-like fashion, autophagy-sufficient macrophages predominantly activated apoptotic pathways. Thus, autophagy depletion dramatically alters the mode of cell death during *M. tuberculosis* infection from apoptosis to necrosis, which promotes inflammation[27,48,49].

To observe the dynamics of individual macrophages more clearly, we generated high-density time-lapse videos of infected cells. Surprisingly, in addition to increased necrosis (Fig. 6c), we observed an extremely high level of efferocytosis of necrotic cells by uninfected macrophages patrolling the monolayers (Fig. 6d,e and Supplementary Video 3). We were able to observe waves of cells initially dying by necrosis followed by efferocytosis, that then precipitated another wave of rapid cell death of the engulfing cell and its subsequent efferocytosis by yet another macrophage (Fig. 6d). The average time for an infected cell to undergo necrosis was ~15 h (Extended Data Fig. 9c) but the time for a previously uninfected cell to die after efferocytosis of an infected necrotic cell was only 10 h (Extended Data Fig. 9d), highlighting that the infected dead cells induced the death of the phagocytosing cell. Thus, blocking autophagy during infection with *M. tuberculosis* leads to rapid necrosis which, in turn, promotes a chain reaction of efferocytosis and necrotic cell death (Fig. 6f).

Discussion

Our work shows that multiple core autophagy factors are required for defence against *M. tuberculosis* infection in mice. Although the *cre–lox* system is an invaluable tool for genetic studies, there are several important limitations to the technology that complicate comparisons between different floxed genes[25]. In this case, variability in recombination efficiency led to insufficient inhibition of *Atg16L1* and *Atg7* expression in mice. By increasing the efficiency of recombination, we were able to detect sensitivity to *M. tuberculosis* infection. These results mean that research efforts should be refocused on the role of autophagy, including ATG5, in defence against *M. tuberculosis*[13,14]. Our work indicates that progress in understanding the mechanisms by which autophagy limits inflammatory responses and promotes resistance may be key for harnessing this pathway as a potential avenue for host-directed therapeutics and vaccine design to fight tuberculosis[14,16,50,51].

It is important to note that despite the phenotypes uncovered upon increased recombination efficiencies of *Atg7* and *Atg16L1*, similar levels of deletion of *Atg5* consistently led to stronger phenotypes. We envision at least two possible explanations for this difference. First,

as suggested by ref. 13, ATG5 may play an autophagy-independent role in TB resistance. To date, there are at least two reports suggesting an autophagy-independent function of ATG5, both showing that it can regulate cell death pathways[46,52]. In this way, the enhanced phenotype of *Atg5*-depleted mice may be due to the combination of the loss of autophagy and this specialized function. Alternatively, subtle differences in gene inhibition between the different floxed genes may lead to different levels of autophagic flux that may have effects during acute infection. Indeed, the increased recombination in *Atg16L1*$^{fl/fl}$ *LysMcre*$^{+/+}$ mice led to significant decrease in mouse weight at 3 weeks postinfection (Fig. 2b), a phenotype very similar to that of *Atg5*$^{fl/fl}$ *LysMcre*$^{+/+}$ mice (Fig. 2a). Perhaps even slightly stronger inhibition of autophagy would lead to the rapid death like *Atg5*-deficient mice. This is especially pertinent in vivo where variation of *LysMcre* expression[53], recombination, *Atg* mRNA half-life, ATG protein turnover, in combination with the cellular dynamics in infected tissue[54], could all give rise to differences in autophagy levels (and inflammatory necrotic cell death) within lung immune cells between these mouse strains.

Our work shows that autophagy protects *M. tuberculosis*-infected BMMs in culture by limiting ESX-1 mediated access to the cytosol and preventing necrosis. While apoptosis is considered a protective mechanism against tuberculosis[48], necrosis is generally regarded as a detrimental mode of cell death for the host[55,56]. Studies have shown that efferocytosis of apoptotic macrophages infected with *M. tuberculosis* limits bacterial growth[57,58]. However, there is increasing evidence that phagocytosis of necrotic debris differs from the engulfment of apoptotic cells[59]. Indeed, ref. 60 reported that phagocytosis of necrotic neutrophils by macrophages promotes *M. tuberculosis* growth.

In our model, the absence of autophagy leads to necrosis and engulfment by naïve phagocytes, which results in a wave of rapid necrosis that promotes inflammation and infection (Fig. 6f). Whether this mechanism is how autophagy functions to regulate *M. tuberculosis* growth and host inflammatory responses during pulmonary infection remains to be elucidated.

Methods

Mice

All mice were housed in specific pathogen-free conditions and treated using procedures described in an animal care protocol (AUP-2015–11-8096) approved by the Institutional Animal Care and Use Committee of University of California Berkeley, in adherence with guidelines from the Guide for the Care and Use of Laboratory Animals of the National Institutes of Health. The *Atg5*$^{fl/fl}$ *LysMcre*, *Atg7*$^{fl/fl}$ *LysMcre*, *Atg16L1*$^{fl/fl}$ *LysMcre* and all flox control mice were provided by H. W. Virgin at Washington University, St Louis. *LysMcre*$^{+/+}$ mice were generated in our facility by crossing *Atg7*$^{fl/fl}$ *LysMcre* mice to wild-type C57BL/6J mice obtained from Jackson Laboratories.

Macrophages

Primary murine BMMs were prepared by flushing femurs from 10- to 12-week-old female mice. Bone marrow extracts were treated for 5 min with 5 ml of Red Blood Cell lysis buffer

(Gibco) and seeded onto non-treated 15 cm tissue culture plates at 5.0×10^6 cells per plate in 20 ml of DMEM, high glucose (Gibco) supplemented with 10% FBS, 2 mM glutamine (Gibco), 0.11 mg ml^{-1} sodium pyruvate (Gibco) and 10% MCSF derived from 3T3-MCSF cell culture supernatants. Macrophages were given an additional 10 ml of macrophage media on days 3, 6 and 8 and were differentiated for 10 days unless indicated otherwise. All experiments were performed with BMMs collected and differentiated simultaneously.

Bacterial strains and culture

All *M. tuberculosis* strains were grown to log phase in 7H9 liquid media (BD) supplemented with 10% Middlebrook OADC (Sigma), 0.5% glycerol and 0.05% Tween-80 in roller bottles at 37 °C. The Δ*eccC M. tuberculosis* Erdman strain was described previously[38]. The *M. tuberculosis* Erdman strain expressing eGFP under control of the MOP promoter was a gift from S. Stanley's laboratory[61]. *The M. marinum* strain expressing mCherry was grown at 33 °C in 7H9 with 10% OADC, 0.5% glycerol, 0.5% Tween-80.

Mouse infection with *M. tuberculosis*

All animal studies have been approved by the University of California Berkeley Institutional Animal Care and Use Committee (protocol no. AUP-2015–11-8096–2). Male and female mice at 8–12 weeks old were infected with ~100 c.f.u. of exponentially replicating *M. tuberculosis* Erdman using an inhalation exposure system (Glas-Col). Bacterial burden at 24 h postinfection was determined by plating lung homogenates of five mice per infection onto 7H10 plates with polymyxin B (200,000 U l^{-1}), carbenicillin (50 mg l^{-1}), trimethoprim lactate (20 mg l^{-1}) and amphotericin B (5 mg l^{-1}). Plates were incubated at 37 °C in 5% CO_2 for 25 days before counting colonies. For survival experiments, 10–12 mice of each genotype were infected with *M. tuberculosis*, except for *LysMcre*$^{+/+}$ mice (five mice only). Mouse weight was checked weekly and mice were killed after 15% loss of their maximum body weight. For c.f.u., histology and flow cytometry experiments, two to seven mice were killed at days 21 and 70 postinfection. The left lung was homogenized in phosphate-buffered saline (PBS) plus 0.05% Tween-80 and serial dilutions were plated on 7H11 plates supplemented with 10% oleic acid, albumin, dextrose and catalase and 0.5% glycerol. Total c.f.u. were counted 21 days after plating. The right superior lobes were used for histology. Samples were fixed in 10% formalin for at least 48 h then stored in 70% ethanol. Samples were sent to the University of California Davis Center for Genomic Pathology Laboratory for embedding in wax, sectioning and staining with H&E. The extent of lesions was determined on ImageScope by a microscopist blinded to sample identity. The remaining lung lobes were used for flow cytometry analysis.

Flow cytometry

Lung lobes were minced with scissors and a surgical razor and digested with collagenase XI (300 U ml^{-1}) with DNase I for 45 min at 37 °C. Single-cell suspensions were generated by mechanical disruption through a 70 μm cell strainer. Then, red blood cells were lysed by incubation with ACK lysis buffer for 3 min. Cells were resuspended in 10 ml of RPMI supplemented with 10% FBS. Dead cells were excluded using a fixable live/dead stain. Cells were fixed with 4% paraformaldehyde and samples were taken out of the BSL3 laboratory. All stains were carried out in PBS containing 2% FBS (v/v) including anti-CD16/32 Fc

blocking and normal mouse serum. Cells were stained for 30 min at 4 °C with the following antibodies: CD11b M1–70, CD11c N418, Ly6G 1A8, Ly6C H1.4, CD8 53–6.7, B220 RA3–6B2, CD64 X54–5/7.1, SiglecF E50–2440, MHCII M5/114.15.2 (BioLegend), CD90.2 53–2.1, MerTK DS5M-MER (eBio), CD4 GK1.5 (BD Horizon), CD44 IM7 and NK1.1 PK136 (BD Biosciences). All cells were analysed on a LSR Fortessa (BD Biosciences) and data were analysed with FlowJo. Gating strategy is displayed in Extended Data Fig. 2.

Macrophage infection with *M. tuberculosis*

For all experiments, differentiated macrophages were seeded 48 h before infection and incubated at 37 °C with 5% CO_2. Macrophages were infected with *M. tuberculosis* as previously described[62]. Briefly, *M. tuberculosis* was grown to logarithmic phase and washed twice with PBS. Aggregates were removed by centrifugation at 200*g* and sonication. Then, bacteria were resuspended in DMEM with 10% horse serum for opsonization. Macrophage monolayers were overlaid with bacterial suspensions and infected at a multiplicity of infection (MOI) of 2 using a 'spinfection protocol' during which cells and bacteria were centrifuged for 10 min at 400*g*. Cells were returned to regular macrophage media. Media were replaced daily for all experiments, except for live imaging assays.

Genotyping and measurement of *cre–lox* recombination efficiency

Cells from bone marrow extracts were seeded onto non-treated 10 cm tissue culture plates at 2.0×10^6 cells per plate and collected after 7, 10 or 12 days of differentiation. Cells were lifted from the plate using PBS with EDTA, centrifuged and cell pellets were conserved at −20 °C until processed. DNA was isolated using a DNeasy blood and tissue kit (Qiagen). The *Atg5* gene was amplified as previously described[63] with the primers exon 3–1 (5′-GAATATGAAGGCACACCCCTGA AATG-3′), short2 (5′-GTACTGCATAATGGT TTAACTCTTGC-3′), check2 (5′-ACAACGTCGAGCACAGCTGCGCAAGG-3′) and 5L2 (5′-CAGG GAATGGTGTCTCCCAC-3′). The *Atg16L1* gene was amplified with the primers F5 (5′-CTTTCTCAACAGAACCAGCAGTAC-3′), R4 (5′-GT AGAAAGACTGGTGATGGTAAACC-3′) and Del3 (5′-AGAAGT GCCTGTGGGTGGGT-3′)[64]. The *Atg7* gene was amplified as previously described[65] with primers Hind-Fw (5′-TGGCTGCTACTTCTGCAATGATGT -3′), *Atg7* ex14 F (5′-TCTCCCAAGACAAGACAGGGTGAA-3′), Pst-Rv (5′-CAGGACAGAGACCATCAGCTCCAC-3′) and *Atg7* ex14 R (5′-AAGCCAAAGGAAACCAAGGGAGTG-3′). In all cases, touchdown PCR was used (94 °C (4 min); 12 cycles of 94 °C (30 s), 72 °C (30 s)—1 °C per cycle, 72 °C (1 min); 30 cycles of 94 °C (30 s), 60 °C (30 s), 72 °C (1 min); 72 °C (5 min)).

Measurement of mRNA levels of autophagy genes

The 3.0×10^6 macrophages differentiated for 10 days were lifted from culture plates using PBS with EDTA, centrifuged and resuspended in 1 ml of Trizol reagent (Life Technologies). Trizol cell suspensions were stored at −80 °C until further analysis. A total of 200 µl of chloroform were added to Trizol cell suspensions. Samples were centrifuged at 15,000*g* for 10 min at 4 °C. The aqueous fraction was isolated and an equal volume of 70% ethanol was added. RNA was purified using a RNeasy total RNA kit (Qiagen). Purified RNA samples were treated with DNase (Purelink) and EDTA. First-

strand complementary DNA was generated using the SuperScript III First-Strand Synthesis System (Invitrogen) with 50 ng of RNA template and random hexamer primers. RNA template was removed by digestion with RNase H after first-strand synthesis. Quantitative PCR was performed using the CFX Connect Real-Time PCR System (Bio-Rad) with iTaq Universal SYBR Green Supermix (Bio-Rad) according to the manufacturer's specifications. Primers for the autophagy genes were designed to span the exon junction that precedes the exon flanked by LoxP sites to prevent detection of a truncated version of the mRNA (exons 2–3 for *Atg5*, exons 2–3 for *Atg16L1* and exons 13–14 for *Atg7*). All transcript levels were normalized to the housekeeping gene *Actb*. The following primers were used in this study: *Atg5* exon 2 sense—5′-TGTGGTTTGGACGAATTCCAACTTG-3′; *Atg5* exon 3 antisense—5′-CAACGTCAAATAGCTGACTCTTGGC-3′; *Atg16L1* exon 2 sense—5′-CTACAAGCAGAAAAGCATGACATGCC-3′; *Atg16L1* exon 3 antisense—5′-CAGCTCTTCCTGGTGTTTGATCCTC-3′; *Atg7* exon 14 sense—5′-GGCTGCTACTTCTGCAATGATGTG-3′; *Atg7* exon 15 antisense—5′-GGACAGAGACCATCAGCTCCAC-3′; *Actin* sense—5′-GAAGTCCCTCACCCTCCCAA-3′; and *Actin* antisense—5′-GGCATGGACGCGACCA-3′.

Western blot

A total of 1.0×10^6 macrophages were cultured overnight in six-well non-tissue culture treated plates. On the next day, cells were incubated for 8 h with either fresh media or EBSS. For the EBSS treatment, 300 nM balofilomycin were added 2 h before the end of the treatment. Cells were lysed with RIPA buffer supplemented with complete protease inhibitor cocktail (Roche). Protein concentration of the lysates was determined with a Micro-BCA kit (Thermofisher). A total of 15 μg of protein lysate were separated by SDS–polyacrylamide gel electrophoresis (Bio-Rad Miniprotean TGX 4–20%) and transferred onto PVDF membranes. After blocking with Odyssey blocking buffer, LC3 conversion was probed using mouse anti-LC3 (Sigma L7543, dilution 1:1000). Anti-ß-actin rabbit monoclonal (Cell Signaling β-Actin D6A8, dilution 1:1,000) was used as a loading control. Membranes were imaged on an Odyssey scanner (Li-cor). Band intensities were quantified using ImageJ (National Institutes of Health).

Live imaging of macrophage infections

BMMs were seeded at a density of 1.2×10^5 cells per well in 24-well glass bottom plates (Cellvis) and infected at an MOI of 2 with *M. tuberculosis* Erdman or *M. tuberculosis* Erdman expressing eGFP. Images were acquired every 30 min or 1 h for 8 days with a BZ-X710 microscope (Keyence, ×20 objective) equipped with a temperature and CO_2 control chamber (Tokai Hit). Media were not replaced during the experiment. For cell death measurement, 0.1 μg ml^{-1} of PI (Life Technologies) and two drops per millilitre of CellEvent Caspase-3/7 Green ReadyProbes reagent (Invitrogen) were added to the media at the beginning of the infection to measure necrosis and apoptosis, respectively. The number of PI and CellEvent-positive cells was quantified with ImageJ. Briefly, all images were combined into a single stack of images. All images were binarized using the same threshold and the number of PI-positive or CellEvent-positive puncta was automatically quantified for each time point using the Analyze Particles module.

Quantification of cell death and bacterial growth during macrophage infection

Macrophages were seeded at 1.0×10^5 cells per well in a non-tissue culture treated 48-well plate (Corning) and infected with *M. tuberculosis* Erdman expressing eGFP at an MOI of 1. Each condition was performed in technical triplicates and eight images per well were acquired on an ImageXpress micro 4 high-content microscope (Molecular Devices). Media were replaced every day and cells were imaged daily (that is, the same samples were imaged repeatedly) until all cells appeared dead by their morphologic appearance. The number of live macrophages and the mean fluorescence intensity of the bacteria were quantified using the MetaXpress software (Molecular Devices). Individual cells and bacterial aggregates were both detected and quantified using the 'find object' module on the brightfield channel and the GFP channel, respectively. For infections with Δ*eccC M. tuberculosis* Erdman, media changes and imaging of the cells were performed every other day until all cells appeared dead.

Actin tail formation

Macrophages were seeded at a density of 1.5×10^5 cells per well in 24-well plate containing glass coverslips and infected with *M. marinum* overexpressing mCherry at an MOI of 2. Infected cells were incubated at 33 °C with 5% CO_2 for 11 h then fixed with 4% paraformaldehyde for 15 min. Then, coverslips were incubated for 30 min in permeabilization/blocking buffer (PB buffer: PBS containing 5% fetal bovine serum and 0.05% saponin (Sigma Aldrich)). Coverslips were incubated for 30 min with phalloidin AlexaFluor-488 (Invitrogen; no. A12379; 1:200 dilution) and Hoechst (Invitrogen, diluted 1:10,000) diluted in PB buffer, then washed three times with PBS before mounting in a drop of ProLong Gold antifade reagent (Invitrogen). Imaging was performed with a KEYENCE BZ-X700 fluorescent microscope using a ×60 objective. The percentage of bacteria with actin tails was scored on ImageJ (National Institutes of Health) by a microscopist blinded to sample identity. A minimum of 300 bacteria were quantified for each condition.

Measurement of mode and time of cell death

Atg5$^{fl/fl}$ *LysMcre*$^{+/+}$ macrophages were infected and imaged as described in the section Live imaging of macrophage infections. A total of 145 infected macrophages from three independent experiments were manually tracked using ImageJ. For each cell, the occurrence of 'efferocytosis' or 'cell death' events were recorded. Timing of each event is displayed in Extended Data Fig. 9c,d.

Extended Data

a

		13bp	8bp spacer	13bp
Wild-type	LoxP	ATAACTTCGTATA	NNNTANNN	ATAACTTCGTATA
Atg5	LoxP site 1	ATAACTTCGTATA	ATGTATGC	ATAACTTCGTATA
Atg5	LoxP site 2	ATAACTTCGTATA	ATGTATGC	ATAACTTCGTATA
Atg16L1	LoxP site 1	ATAACTTCGTATA	GCATACAT	ATAACTTCGTATA
Atg16L1	LoxP site 2	ATAACTTCGTATA	GCATACAT	ATAACTTCGTATA
Atg7	LoxP site 1	ATAACTTCGTATA	ATGTATGC	ATAACTTCGTATA
Atg7	LoxP site 2	ATAACTTCGTATA	ATGTATGC	ATAACTTCGTATA

b

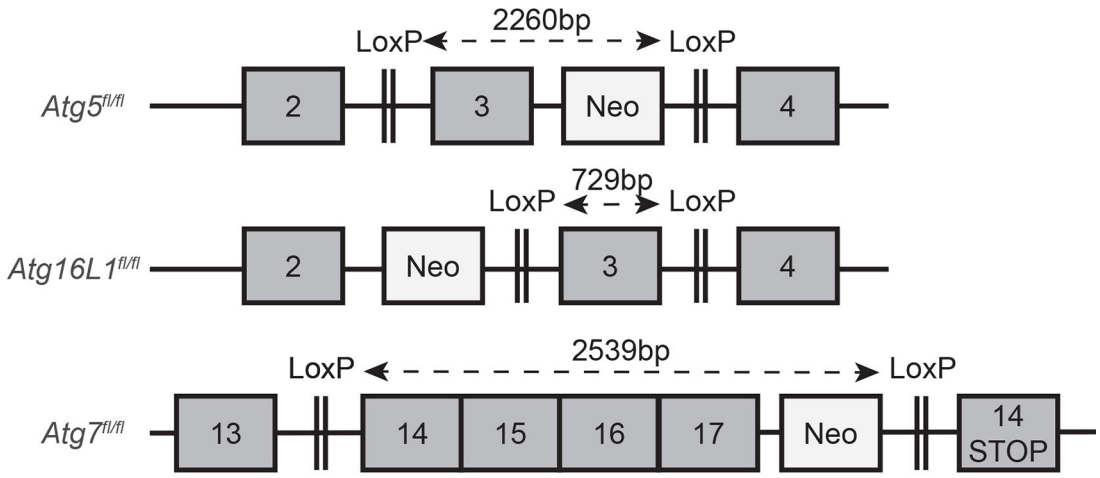

c

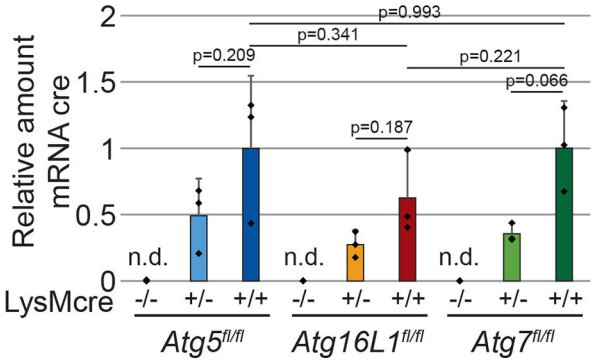

Extended data Fig. 1. Sequences of LoxP sites, map of LoxP site insertions and measurement of Cre expression levels.

a, Sequences of LoxP sites in *Atg5*$^{fl/fl}$, *Atg16L1*$^{fl/fl}$ and *Atg7*$^{fl/fl}$ mice. **b**, Map of LoxP sites and Neomycin resistance cassettes insertions in *Atg5*$^{fl/fl}$, *Atg16L1*$^{fl/fl}$ and *Atg7*$^{fl/fl}$ mice. Grey boxes denote exons. **c**, Measurement of mRNA levels of Cre in bone marrow-derived macrophages differentiated for 10 days. Results are the means ± SD from 3 biological replicates. n.d. = not detected. Statistical analysis performed with two-sided t-test.

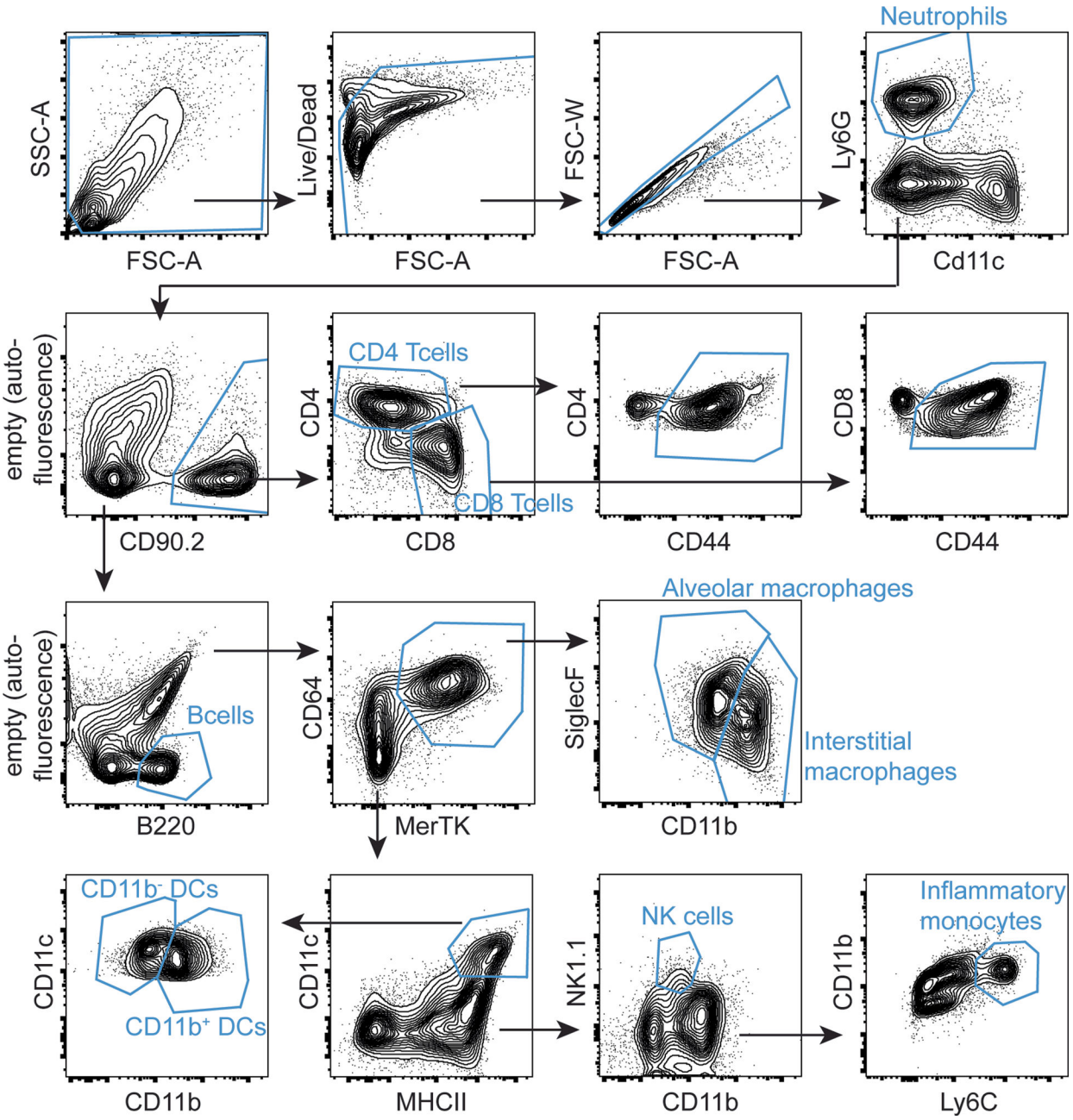

Extended data Fig. 2. Gating strategy used to isolate lung populations in *M. tuberculosis*-infected mice.

Lungs from infected mice were harvested after 21 or 70 days of infection. Single cells from lung homogenates were sorted into different immune cell populations according to the strategy outlined in this figure.

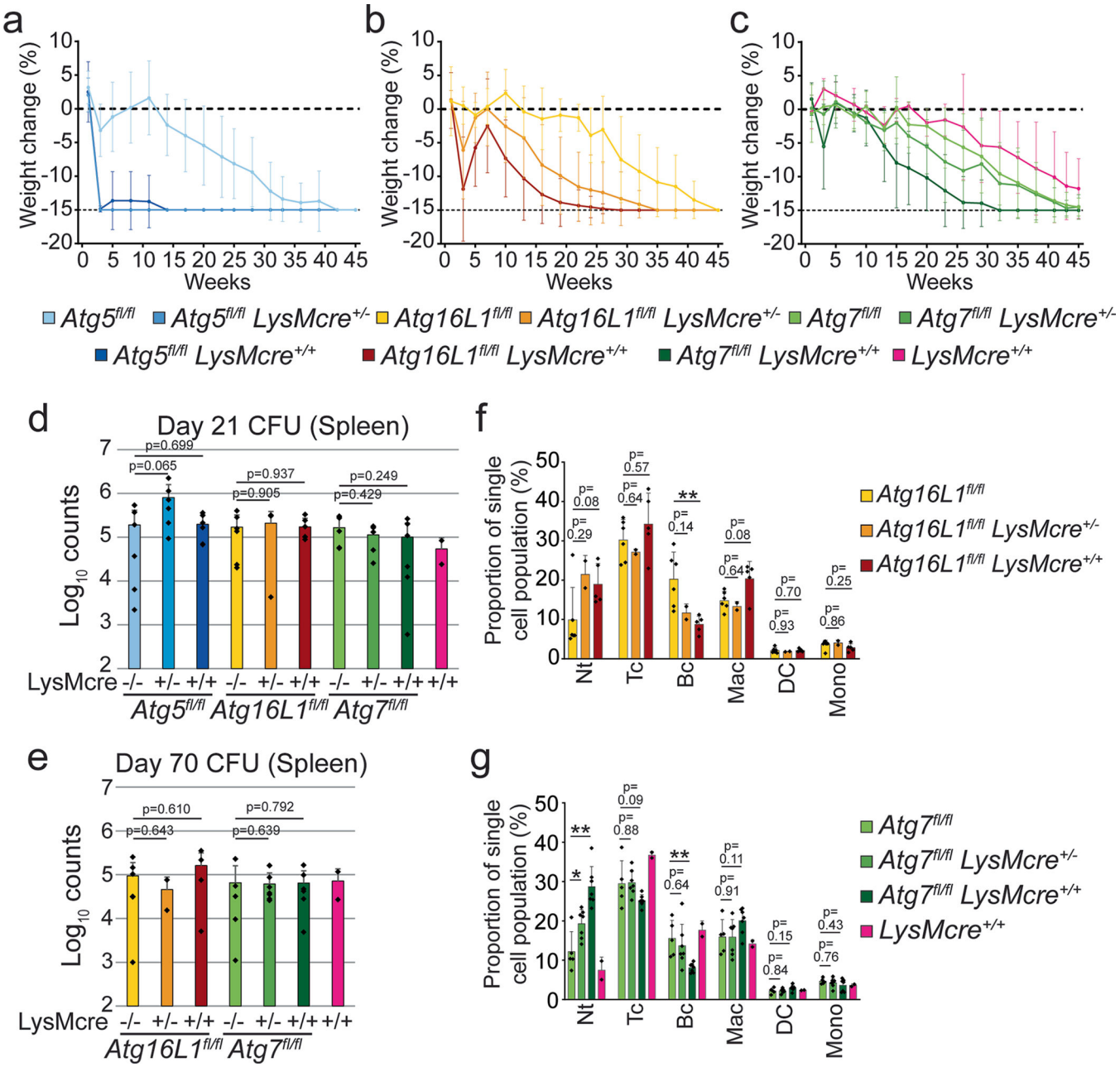

Extended data Fig. 3. Additional in vivo data on autophagy mutant mice infected with *M. tuberculosis*.

a-c, Mice (n=12–17 per group) were infected with approximately 100 colony-forming units (c.f.u.) of *M. tuberculosis* and tracked for weight change (**a-c**). Data is presented as means ± SD. Mice that lost 15% body weight were sacrificed are counted at -15% for subsequent time points. **d-e**, CFU counts from the lungs of mice (n=5 per group) infected with approximately 100 c.f.u of *M. tuberculosis*. Spleens were harvested at 21 days post infection (**d**) or 70 days post infection (**e**). Data is presented as means ± SD. **f-g**, Proportion of immune cell populations in the lungs of *Atg7* (**f**) and *Atg16L1* (**g**) mutant mice infected for 70 days with *M. tuberculosis*. Results are the means ± SD from 2–7 mice

per condition. Nt = Neutrophils, Tc = T cells, Bc = B cells, Mac = Macrophages, DC = Dendritic cells, Mono = Ly6Chi inflammatory monocytes. For statistical analysis for CFU and histology experiments, *LysM*cre$^{+/-}$ and *LysM*cre$^{+/+}$ conditions were compared to the respective *LysM*$^{wt/wt}$ control. * P ≤ 0.05, ** P ≤ 0.01 by two-sided Mann Whitney test.

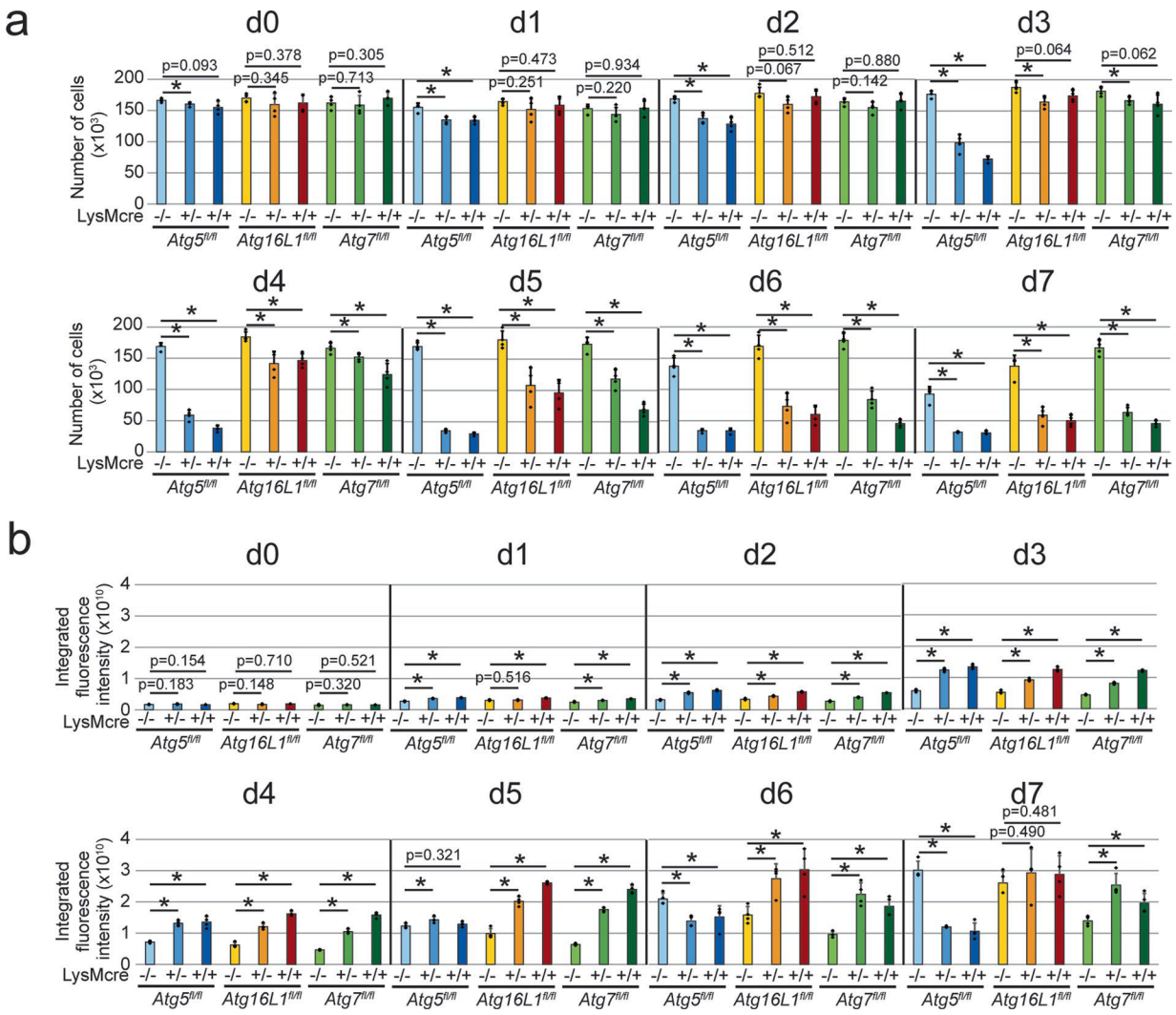

Extended data Fig. 4. Statistics of cell death and *M. tuberculosis* growth during time-course macrophage infection with *M. tuberculosis*.

a-b, Same data as in Fig. 4b–c but each day is presented as an individual graph. Data represents number of macrophages (**a**) and Mean Fluorescent Intensity of fluorescent bacteria (**b**). Results are the means ± SD from 4 technical replicates. For statistical analysis, *LysM*cre$^{+/-}$ and *LysM*cre$^{+/+}$ conditions were compared to the respective *LysM*$^{wt/wt}$ control. * P ≤ 0.05 by two-sided t-test/.

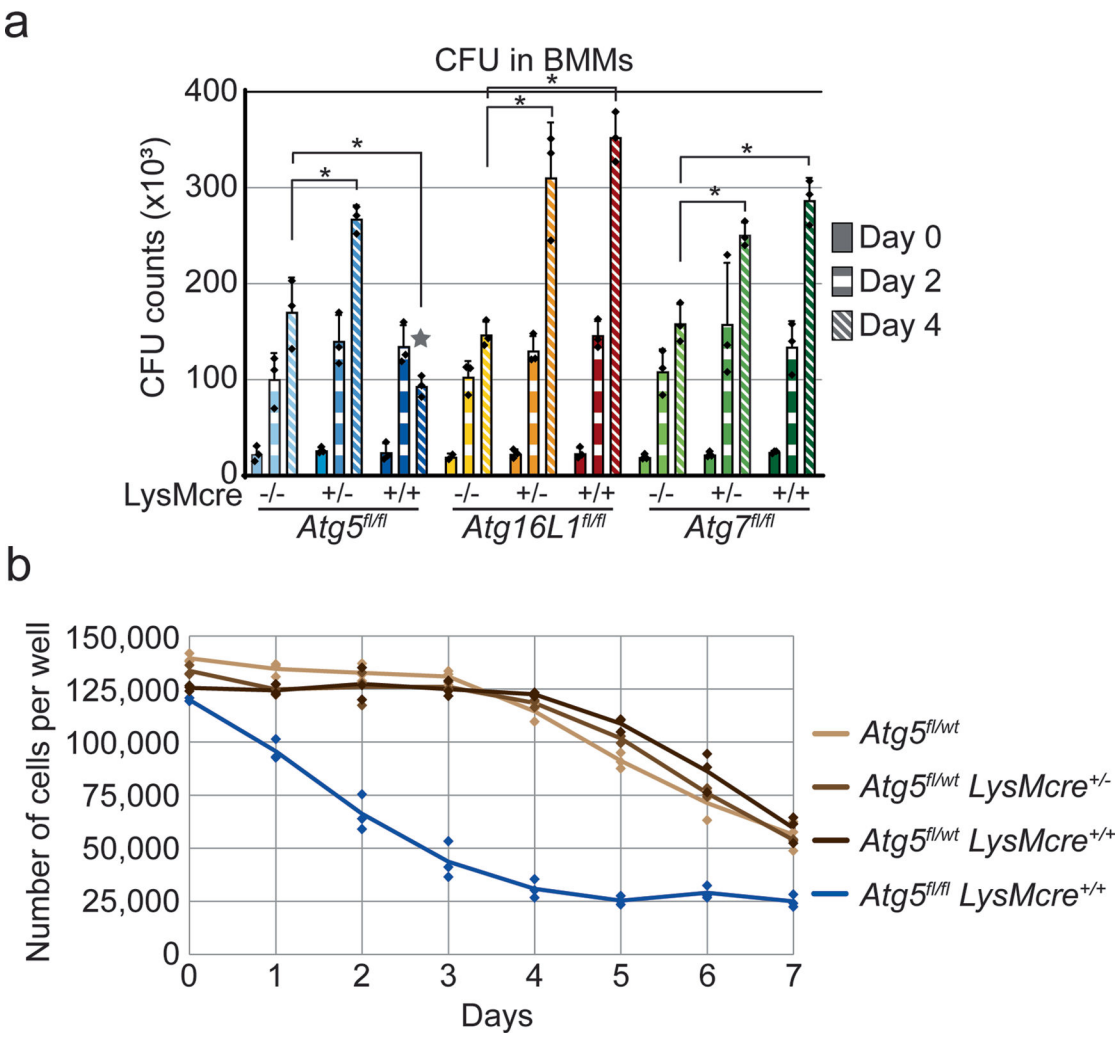

Extended data Fig. 5. Growth of *M. tuberculosis* in autophagy-mutant BMMs and susceptibility of *Atg5*-flox hemizygous macrophages.

a, BMMs from autophagy mutant mice were infected with *M. tuberculosis* at a MOI of 2. CFU were enumerated at day 0, day 2 and day 4 post infection. Results are the means ± SD from 3 technical replicates per condition. For statistical analysis, *LysM*cre$^{+/-}$ and *LysM*cre$^{+/+}$ conditions were compared to the respective *LysM*$^{wt/wt}$ control for the day 4 condition. * P ≤ 0.05 by two-sided t-test. Grey star denotes conditions were the macrophage monolayer was disrupted. **b**, Macrophages from *Atg5*$^{fl/wt}$, *Atg5*$^{fl/wt}$ *LysM*cre$^{+/-}$, *Atg5*$^{fl/wt}$ *LysM*cre$^{+/+}$ and *Atg5*$^{fl/fl}$ *LysM*cre$^{+/+}$ were infected with *M. tuberculosis* at a MOI of 1 and macrophages were enumerated by imaging every day for 7 days. Macrophages carrying one wild-type allele of *Atg5* and one recombined allele (*Atg5*$^{fl/wt}$ *LysM*cre$^{+/-}$, *Atg5*$^{fl/wt}$ *LysM*cre$^{+/+}$) were indistinguishable from wild-type cells. Each condition was tested in technical triplicates.

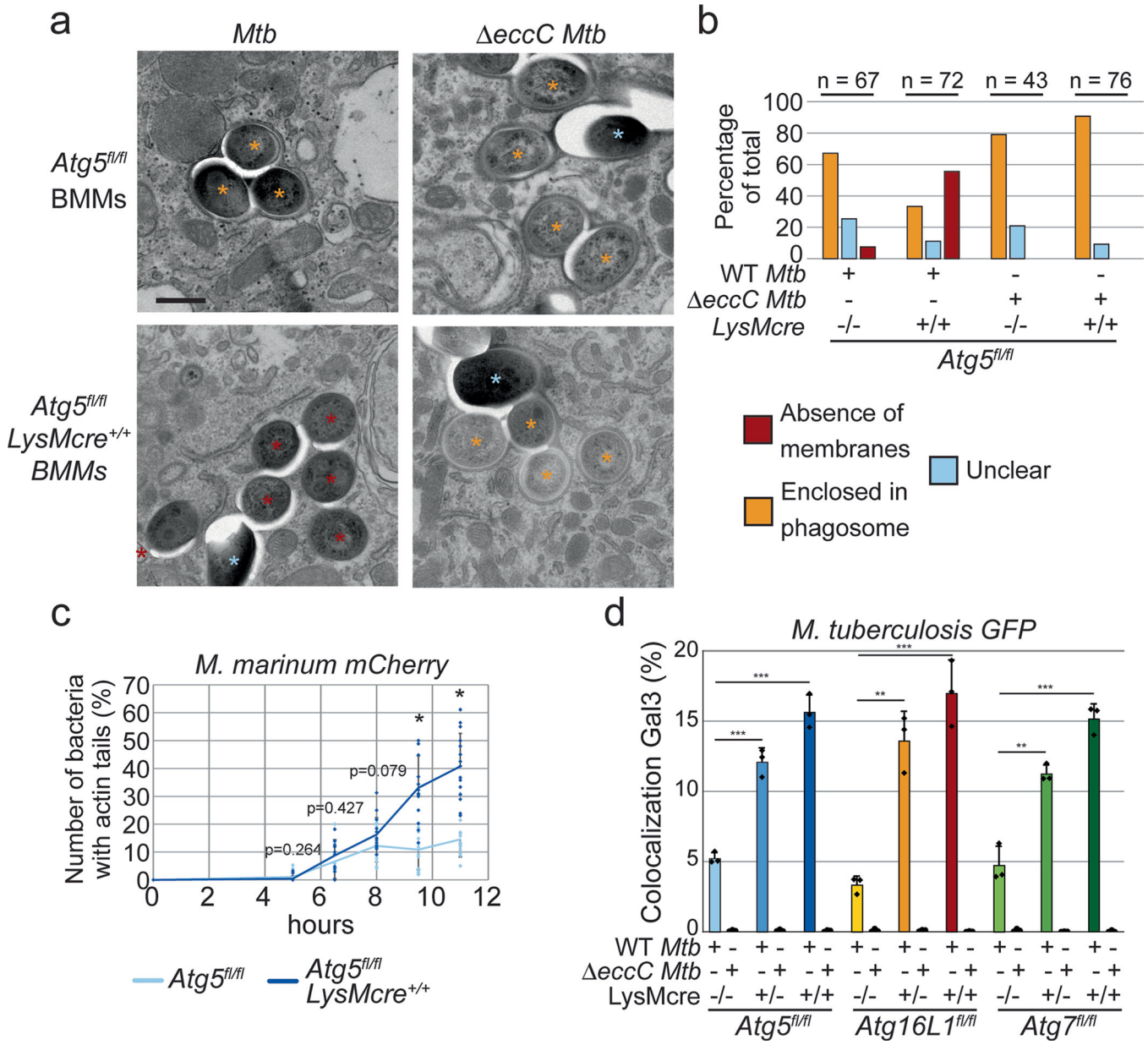

Extended data Fig. 6. Absence of autophagy promotes phagosome escape of Mycobacteria in macrophages.

a, Illustrative images of wild-type or Δ*eccC M. tuberculosis* bacteria in *Atg5*$^{fl/fl}$ or *Atg5*$^{fl/fl}$ *LysM*cre$^{+/+}$ macrophages after 24 hours of infection. Orange asterisks denote bacteria fully enclosed in phagosomes, blue asterisks show bacteria with poor membrane preservation, red asterisks denote bacteria in the cytosol. Scale bar = 0.4 μm. **b**, Quantification of bacteria fully enclosed in phagosomes, present directly in the cytosol, or with poor membrane preservation. Data is from a single experiment. A minimum of 40 bacteria per condition were quantified. **c**, Actin tail formation by *M. marinum* expressing mCherry in *Atg5*$^{fl/fl}$ or *Atg5*$^{fl/fl}$ *LysM*cre$^{+/+}$ macrophages was measured at 6.5h, 8h, 9.5h and 11 hours post infection. Results are the means ± SD for 15 images from two technical replicates. * P ≤ 0.05 by two-sided t-test. d, Autophagy-mutant macrophages were infected with *M.*

tuberculosis expressing GFP or Δ*eccC M. tuberculosis* expressing GFP. Colocalization with Gal-3 was measured at 10h post-infection. Results are the means ± SD from three technical replicates. For statistical analysis, *LysM*cre$^{+/-}$ and *LysM*cre$^{+/+}$ conditions were compared to the respective *LysM*$^{wt/wt}$ control. * P ≤ 0.05, ** P ≤ 0.01, * P ≤ 0.001 by two-sided Mann Whitney test.

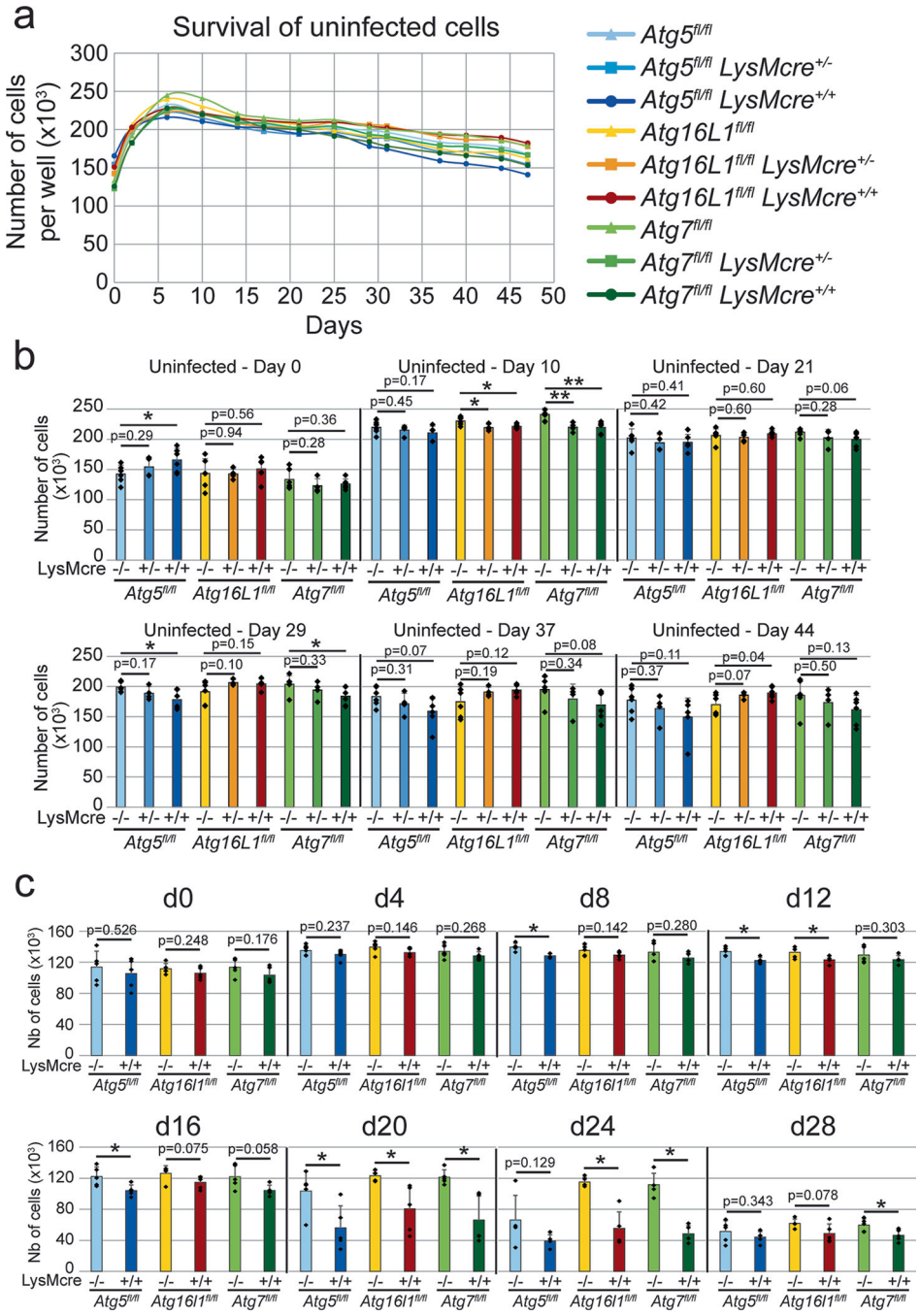

Extended data Fig. 7. Survival of uninfected autophagy-deficient macrophages and statistics of cell death during infection with Δ*eccC M. tuberculosis*.

a-b, Quantification of number of uninfected macrophages over time. Data is averaged from two independent experiments with each condition tested in technical duplicates. Data presented as a time course (**a**) or as selected timepoints for statistical analysis (**b**). Data is presented as means ± SD. **c**, Same data as in Fig. 5c but with selected timepoints presented as an individual graphs. Results are the means ± SD from two independent experiments with each condition tested in technical duplicates. For statistical analysis, number of macrophages in cre-positive conditions were compared to the respective $LysM^{wt/wt}$ control. * $P \leq 0.05$ by two-sided t-test.

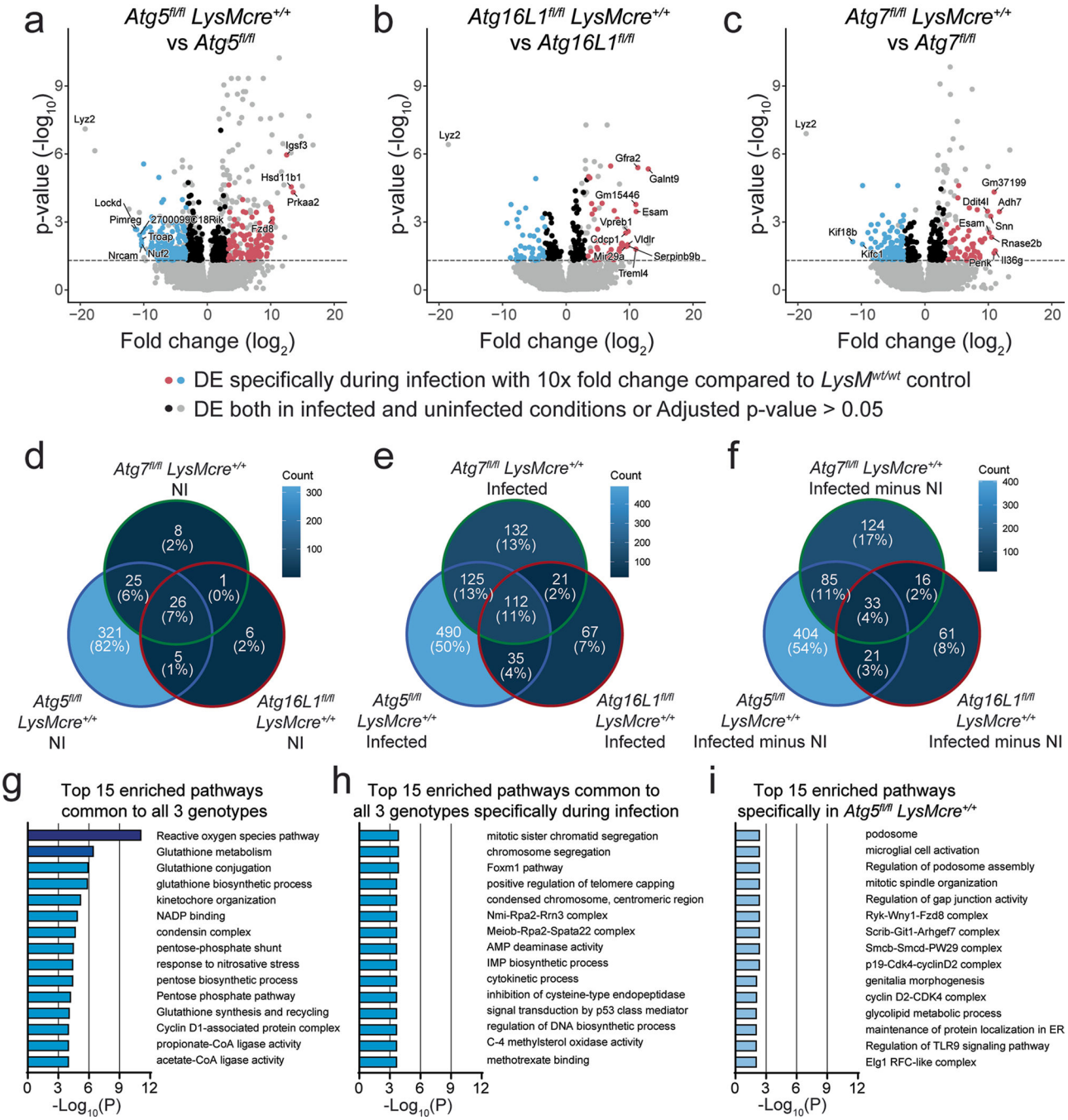

Extended data Fig. 8. RNA-seq on autophagy mutant macrophages infected with *M. tuberculosis*. RNA was collected from uninfected BMMs and BMMs infected with *M. tuberculosis* for 48h.

a-c, Volcano plot showing differentially expressed genes in *Atg5*$^{fl/fl}$ *LysM*cre$^{+/+}$. Grey line demarcates adj.p.value of 0.05. (**a**), *Atg16L1*$^{fl/fl}$ *LysM*cre$^{+/+}$ (**b**) and *Atg7fl/fl LysM*cre$^{+/+}$ (**c**) macrophages compared to their respective flox controls. **d-f**, Venn diagrams showing genes with significant transcriptional changes (adj.p.value ≤ 0.05) for the cre-positive conditions compared to their respective *LysM*$^{wt/wt}$ control. Venn diagram for all DE genes in uninfected conditions (**d**), all DE genes in infected conditions (**e**) and genes exclusively

differentially expressed during infection (i.e. with genes with significant DE in uninfected conditions filtered out) (**f**). **g-i**, Gene enrichment analysis showing pathways enriched in M. tuberculosis-infected cells. Genes with significant transcriptional changes (adj.p.value ≤ 0.05) were used for pathway enrichment using the hypergeometric test (HGT). Datasets for enrichment included: KEGG, REACTOME, MSigDB C2_CP and C3, GO, CORUM, and HALLMARK. Top 15 pathways commonly enriched in *Atg5*$^{fl/fl}$ *LysMcre*$^{+/+}$, *Atg16L1*$^{fl/fl}$ *LysMcre*$^{+/+}$ and *Atg7*$^{fl/fl}$ *LysMcre*$^{+/+}$ (**g**), Top 15 pathways commonly enriched in all 3 genotypes specifically during infection (**h**) and top 15 pathways enriched exclusively in *Atg5*$^{fl/fl}$ *LysMcre*$^{+/+}$ macrophages (**i**).

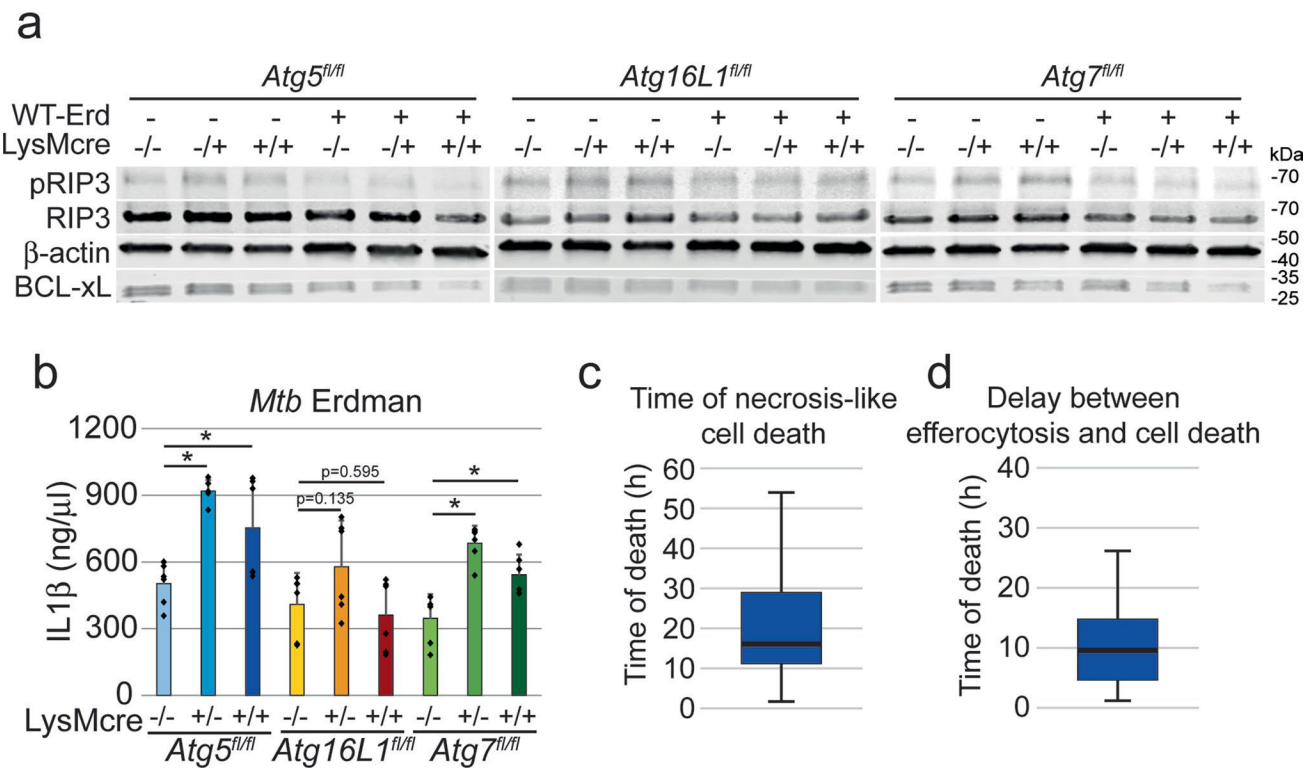

Extended data Fig. 9. *M. tuberculosis* infection induces necrosis-like cell death and efferocytosis in autophagy-deficient macrophages.

a, Western blot for pRIP3, RIP3, BCL-xL and β-actin on cell lysates from uninfected BMMs and BMMs infected for 48 hours with *M. tuberculosis*. **b**, Measurement by ELISA of IL-1β secretion in supernatant of macrophages infected for 48 hours with *M. tuberculosis*. Results are the means ± SD from two independent experiments, in which each condition was tested in technical triplicates. * P ≤ 0.05 by two-sided t-test. **c-d**, *Atg5*$^{fl/fl}$ *LysM*cre$^{+/+}$ macrophages were infected with GFP-expressing *M. tuberculosis* and imaged every 30 minutes over a 6-day period (Supplementary Video 3). Time and mode of cell death were recorded for 145 *Atg5*$^{fl/fl}$ *LysM*cre$^{+/+}$ macrophages infected with GFP-expressing *M. tuberculosis* from 3 independent experiments. The average time of death by necrosis-like cell death (**c**) and the delay between efferocytosis and subsequent cell death (**d**) were measured. Center line: median; box limits: upper and lower quartiles; whiskers: 1.5x interquartile range. n = 80 and 65, respectively.

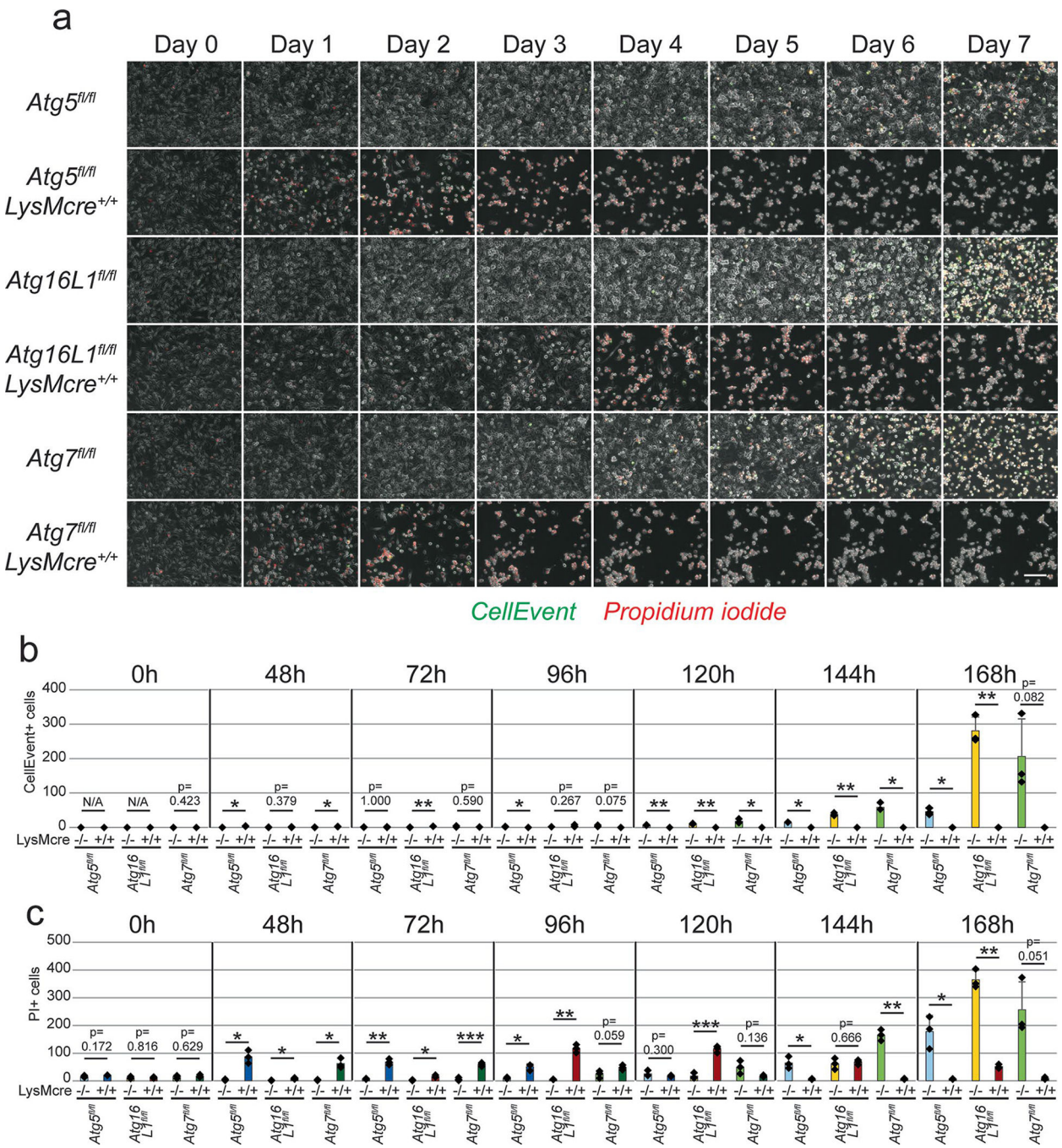

Extended data Fig. 10. Illustrative images and statistics of PI and CellEvent staining of macrophages infected with *M. tuberculosis*.

a, Illustrative images of experiment quantified in **Fig. 6a–b**. Autophagy-deficient macrophages were infected with *M. tuberculosis* at a MOI of 1. Propidium iodide and CellEvent Caspase-3/7 reagent were added to the media at the beginning of the infection. Cells were imaged every 30 minutes over a period of 8 days. Scale bar denotes 100 μm. **b**, Same data as in **Fig. 6a–b** but with selected timepoints presented as an individual graphs. Results are the means ± SD with each condition tested in technical triplicates. For

statistical analysis, number of CellEvent (**b**) and propodium iodide (**c**) positive macrophages in cre-positive conditions were compared to the respective *LysM*$^{wt/wt}$ control. * $P \leq 0.05$, ** $P \leq 0.01$, * $P \leq 0.001$ by two-sided t-test.

Supplementary Material

Refer to Web version on PubMed Central for supplementary material.

Acknowledgements

We acknowledge members of the Cox, Stanley, Vance and Portnoy laboratories for helpful discussion. We thank D. A. Portnoy (University of California Berkeley) for graciously letting us use his Keyence microscope. We thank H. W. Virgin (Washington University) for providing all the mouse lines used in this study. We thank the staff of the Office of Laboratory Animal Care of the University of California Berkeley for the care provided to the animals used in this study. We thank the staff at the University of California Berkeley Electron Microscope Laboratory for advice and assistance in electron microscopy sample preparation and data collection. The sequencing for RNA-seq was carried out at the DNA Technologies and Expression Analysis Cores at the University of California Davis Genome Center, supported by NIH Shared Instrumentation grant 1S10OD010786-01. Embedding in wax, sectioning and staining for histology was performed at the University of California Davis Center for Genomic Pathology Laboratory. This work was supported by NIH grants AI162583 and AI063302 and National Institute of Allergy and Infectious Diseases Host Pathogen Map Initiative grant U19AI135990 (J.S.C.).

Data availability

RNA-seq data can be accessed on the GEO database, accession number GSE226503 (https://www.ncbi.nlm.nih.gov/geo/). All other data are available in the main text, source data, Extended Data figures or Supplementary Information. Source data are provided with this paper.

References

1. Levine B & Kroemer G Biological functions of autophagy genes: a disease perspective. Cell 176, 11–42 (2019). [PubMed: 30633901]
2. Chang C, Jensen LE & Hurley JH Autophagosome biogenesis comes out of the black box. Nat. Cell Biol. 23, 450–456 (2021). [PubMed: 33903736]
3. Deretic V & Lazarou M A guide to membrane atg8ylation and autophagy with reflections on immunity. J. Cell Biol. 221, e202203083 (2022). [PubMed: 35699692]
4. Lu Q et al. Homeostatic control of innate lung inflammation by Vici syndrome gene Epg5 and additional autophagy genes promotes influenza pathogenesis. Cell Host Microbe 19, 102–113 (2016). [PubMed: 26764600]
5. Park S et al. Autophagy genes enhance murine gammaherpesvirus 68 reactivation from latency by preventing virus-induced systemic inflammation. Cell Host Microbe 19, 91–101 (2016). [PubMed: 26764599]
6. Martinez J et al. Noncanonical autophagy inhibits the autoinflammatory, lupus-like response to dying cells. Nature 533, 115–119 (2016). [PubMed: 27096368]
7. Thurston TLM, Wandel MP, Muhlinen N, von, Foeglein, Á. & Randow, F. Galectin 8 targets damaged vesicles for autophagy to defend cells against bacterial invasion. Nature 482, 414–418 (2012). [PubMed: 22246324]
8. Jia J et al. AMPK, a regulator of metabolism and autophagy, is activated by lysosomal damage via a novel galectin-directed ubiquitin signal transduction system. Mol. Cell 77, 951–969 (2020). [PubMed: 31995728]
9. Global Tuberculosis Report 2020 (World Health Organization, 2020).
10. Huang L, Nazarova EV & Russell DG *Mycobacterium tuberculosis*: bacterial fitness within the host macrophage. Microbiol. Spectr. 10.1128/microbiolspec.BAI-0001-2019 (2019).

11. Mayer-Barber KD et al. Host-directed therapy of tuberculosis based on interleukin-1 and type I interferon crosstalk. Nature 511, 99–103 (2014). [PubMed: 24990750]
12. Gutierrez MG et al. Autophagy is a defense mechanism inhibiting BCG and *Mycobacterium tuberculosis* survival in infected macrophages. Cell 119, 753–766 (2004). [PubMed: 15607973]
13. Kimmey JM et al. Unique role for ATG5 in neutrophil-mediated immunopathology during *M. tuberculosis* infection. Nature 528, 565–569 (2015). [PubMed: 26649827]
14. Behar SM & Baehrecke EH Tuberculosis: autophagy is not the answer. Nature 528, 482–483 (2015). [PubMed: 26649822]
15. Watson RO, Manzanillo PS & Cox JS Extracellular *M. tuberculosis* DNA targets bacteria for autophagy by activating the host DNA-sensing pathway. Cell 150, 803–815 (2012). [PubMed: 22901810]
16. Castillo EF et al. Autophagy protects against active tuberculosis by suppressing bacterial burden and inflammation. Proc. Natl Acad. Sci. USA 109, E3168–E3176 (2012). [PubMed: 23093667]
17. Wallis RS & Hafner R Advancing host-directed therapy for tuberculosis. Nat. Rev. Immunol. 15, 255–263 (2015). [PubMed: 25765201]
18. McCubbrey AL, Allison KC, Lee-Sherick AB, Jakubzick CV & Janssen WJ Promoter specificity and efficacy in conditional and inducible transgenic targeting of lung macrophages. Front. Immunol. 8, 1618 (2017). [PubMed: 29225599]
19. Vooijs M, Jonkers J & Berns A A highly efficient ligand-regulated Cre recombinase mouse line shows that LoxP recombination is position dependent. EMBO Rep. 2, 292–297 (2001). [PubMed: 11306549]
20. Heffner CS et al. Supporting conditional mouse mutagenesis with a comprehensive cre characterization resource. Nat. Commun. 3, 1218 (2012). [PubMed: 23169059]
21. Thomson JG, Rucker EB & Piedrahita JA Mutational analysis of loxP sites for efficient Cre-mediated insertion into genomic DNA. Genesis 36, 162–167 (2003). [PubMed: 12872248]
22. Klionsky DJ et al. Guidelines for the use and interpretation of assays for monitoring autophagy (4th edition). Autophagy 17, 1–382 (2021). [PubMed: 33634751]
23. Ji DX et al. Type I interferon-driven susceptibility to Mycobacterium tuberculosis is mediated by IL-1Ra. Nat. Microbiol. 4, 2128–2135 (2019). [PubMed: 31611644]
24. Moreira-Teixeira L et al. Type I IFN exacerbates disease in tuberculosis-susceptible mice by inducing neutrophil-mediated lung inflammation and NETosis. Nat. Commun. 11, 5566 (2020). [PubMed: 33149141]
25. Schmidt-Supprian M & Rajewsky K Vagaries of conditional gene targeting. Nat. Immunol. 8, 665–668 (2007). [PubMed: 17579640]
26. Pépin G et al. Cre-dependent DNA recombination activates a STING-dependent innate immune response. Nucleic Acids Res. 44, 5356–5364 (2016). [PubMed: 27166376]
27. Queval CJ, Brosch R & Simeone R The macrophage: a disputed fortress in the battle against *Mycobacterium tuberculosis*. Front. Microbiol. 8, 2284 (2017). [PubMed: 29218036]
28. Mahamed D et al. Intracellular growth of Mycobacterium tuberculosis after macrophage cell death leads to serial killing of host cells. eLife 6, e22028 (2017). [PubMed: 28130921]
29. Lerner TR et al. *Mycobacterium tuberculosis* replicates within necrotic human macrophages. J. Cell Biol. 216, 583–594 (2017). [PubMed: 28242744]
30. Tan JMJ et al. An ATG16L1-dependent pathway promotes plasma membrane repair and limits *Listeria monocytogenes* cell-to-cell spread. Nat. Microbiol. 3, 1472–1485 (2018). [PubMed: 30478389]
31. Jia J et al. Galectin-3 coordinates a cellular system for lysosomal repair and removal. Dev. Cell 52, 69–87 (2019). [PubMed: 31813797]
32. López-Jiménez AT et al. The ESCRT and autophagy machineries cooperate to repair ESX-1-dependent damage at the *Mycobacterium*-containing vacuole but have opposite impact on containing the infection. PLoS Pathog. 14, e1007501 (2018). [PubMed: 30596802]
33. Houben D et al. ESX-1-mediated translocation to the cytosol controls virulence of mycobacteria. Cell Microbiol. 14, 1287–1298 (2012). [PubMed: 22524898]

34. Simeone R et al. Phagosomal rupture by *Mycobacterium tuberculosis* results in toxicity and host cell death. PLoS Pathog. 8, e1002507 (2012). [PubMed: 22319448]
35. Smith J et al. Evidence for pore formation in host cell membranes by ESX-1-secreted ESAT-6 and its role in *Mycobacterium marinum* escape from the vacuole. Infect. Immun. 76, 5478–5487 (2008). [PubMed: 18852239]
36. Conrad WH et al. Mycobacterial ESX-1 secretion system mediates host cell lysis through bacterium contact-dependent gross membrane disruptions. Proc. Natl Acad. Sci. USA 114, 1371–1376 (2017). [PubMed: 28119503]
37. Bell SL, Lopez KL, Cox JS, Patrick KL & Watson RO Galectin-8 senses phagosomal damage and recruits selective autophagy adapter TAX1BP1 to control *Mycobacterium tuberculosis* infection in macrophages. Mbio 12, e01871–20 (2021).
38. Rosenberg OS et al. Substrates control multimerization and activation of the multi-domain ATPase motor of type VII secretion. Cell 161, 501–512 (2015). [PubMed: 25865481]
39. Stanley SA, Johndrow JE, Manzanillo P & Cox JS The Type I IFN response to infection with *Mycobacterium tuberculosis* requires ESX-1-mediated secretion and contributes to pathogenesis. J. Immunol. 178, 3143–3152 (2007). [PubMed: 17312162]
40. Watson RO et al. The cytosolic sensor cGAS detects *Mycobacterium tuberculosis* DNA to induce type I interferons and activate autophagy. Cell Host Microbe 17, 811–819 (2015). [PubMed: 26048136]
41. Beckwith KS et al. Plasma membrane damage causes NLRP3 activation and pyroptosis during *Mycobacterium tuberculosis* infection. Nat. Commun. 11, 2270 (2020). [PubMed: 32385301]
42. Lim J-A, Zare H, Puertollano R & Raben N $Atg5^{flox}$-derived autophagy-deficient model of Pompe disease: does it tell the whole story? Mol. Ther. Methods Clin. Dev. 7, 11–14 (2017). [PubMed: 29057281]
43. Koo IC et al. ESX-1-dependent cytolysis in lysosome secretion and inflammasome activation during mycobacterial infection. Cell Microbiol. 10, 1866–1878 (2008). [PubMed: 18503637]
44. Wassermann R et al. *Mycobacterium tuberculosis* differentially activates cGAS- and inflammasome-dependent intracellular immune responses through ESX-1. Cell Host Microbe 17, 799–810 (2015). [PubMed: 26048138]
45. Mayer-Barber KD et al. Cutting edge: caspase-1 independent IL-1β production is critical for host resistance to *Mycobacterium tuberculosis* and does not require TLR signaling in vivo. J. Immunol. 184, 3326–3330 (2010). [PubMed: 20200276]
46. Yousefi S et al. Calpain-mediated cleavage of Atg5 switches autophagy to apoptosis. Nat. Cell Biol. 8, 1124–1132 (2006). [PubMed: 16998475]
47. Zhao X et al. Bcl-xL mediates RIPK3-dependent necrosis in *M. tuberculosis*-infected macrophages. Mucosal Immunol. 10, 1553–1568 (2017). [PubMed: 28401933]
48. Behar SM et al. Apoptosis is an innate defense function of macrophages against *Mycobacterium tuberculosis*. Mucosal Immunol. 4, 279–287 (2011). [PubMed: 21307848]
49. Repasy T et al. Bacillary replication and macrophage necrosis are determinants of neutrophil recruitment in tuberculosis. Microbes Infect. 17, 564–574 (2015). [PubMed: 25862076]
50. Paik S, Kim JK, Chung C & Jo E-K Autophagy: a new strategy for host-directed therapy of tuberculosis. Virulence 10, 448–459 (2018). [PubMed: 30322337]
51. Flores-Valdez MA, Segura-Cerda CA & Gaona-Bernal J Modulation of autophagy as a strategy for development of new vaccine candidates against tuberculosis. Mol. Immunol. 97, 16–19 (2018). [PubMed: 29547747]
52. Maskey D et al. ATG5 is induced by DNA-damaging agents and promotes mitotic catastrophe independent of autophagy. Nat. Commun. 4, 2130 (2013). [PubMed: 23945651]
53. Abram CL, Roberge GL, Hu Y & Lowell CA Comparative analysis of the efficiency and specificity of myeloid-Cre deleting strains using ROSA-EYFP reporter mice. J. Immunol. Methods 408, 89–100 (2014). [PubMed: 24857755]
54. Yu Y-RA et al. A protocol for the comprehensive flow cytometric analysis of immune cells in normal and inflamed murine non-lymphoid tissues. PLoS ONE 11, e0150606 (2016). [PubMed: 26938654]

55. Chen M et al. Lipid mediators in innate immunity against tuberculosis: opposing roles of PGE2 and LXA4 in the induction of macrophage death. J. Exp. Med. 205, 2791–2801 (2008). [PubMed: 18955568]
56. Park JS, Tamayo MH, Gonzalez-Juarrero M, Orme IM & Ordway DJ Virulent clinical isolates of *Mycobacterium tuberculosis* grow rapidly and induce cellular necrosis but minimal apoptosis in murine macrophages. J. Leukoc. Biol. 79, 80–86 (2006). [PubMed: 16275894]
57. Divangahi M, Desjardins D, Nunes-Alves C, Remold HG & Behar SM Eicosanoid pathways regulate adaptive immunity to *Mycobacterium tuberculosis*. Nat. Immunol. 11, 751–758 (2010). [PubMed: 20622882]
58. Martin CJ et al. Efferocytosis is an innate antibacterial mechanism. Cell Host Microbe 12, 289–300 (2012). [PubMed: 22980326]
59. Westman J, Grinstein S & Marques PE Phagocytosis of necrotic debris at sites of injury and inflammation. Front. Immunol. 10, 3030 (2020). [PubMed: 31998312]
60. Dallenga T et al. *M. tuberculosis*-induced necrosis of infected neutrophils promotes bacterial growth following phagocytosis by macrophages. Cell Host Microbe 22, 519–530 (2017). [PubMed: 29024644]
61. Sogi KM, Lien KA, Johnson JR, Krogan NJ & Stanley SA The tyrosine kinase inhibitor Gefitinib restricts *Mycobacterium tuberculosis* growth through increased lysosomal biogenesis and modulation of cytokine signaling. ACS Infect. Dis. 3, 564–574 (2017). [PubMed: 28537707]
62. Penn BH et al. An Mtb-human protein–protein interaction map identifies a switch between host antiviral and antibacterial responses. Mol. Cell 71, 637–648 (2018). [PubMed: 30118682]
63. Hara T et al. Suppression of basal autophagy in neural cells causes neurodegenerative disease in mice. Nature 441, 885–889 (2006). [PubMed: 16625204]
64. Hwang S et al. Nondegradative role of Atg5-Atg12/ Atg16L1 autophagy protein complex in antiviral activity of interferon gamma. Cell Host Microbe. 11, 397–409 (2012). [PubMed: 22520467]
65. Komatsu M et al. Impairment of starvation-induced and constitutive autophagy in Atg7-deficient mice. J. Cell Biol. 169, 425–434 (2005). [PubMed: 15866887]

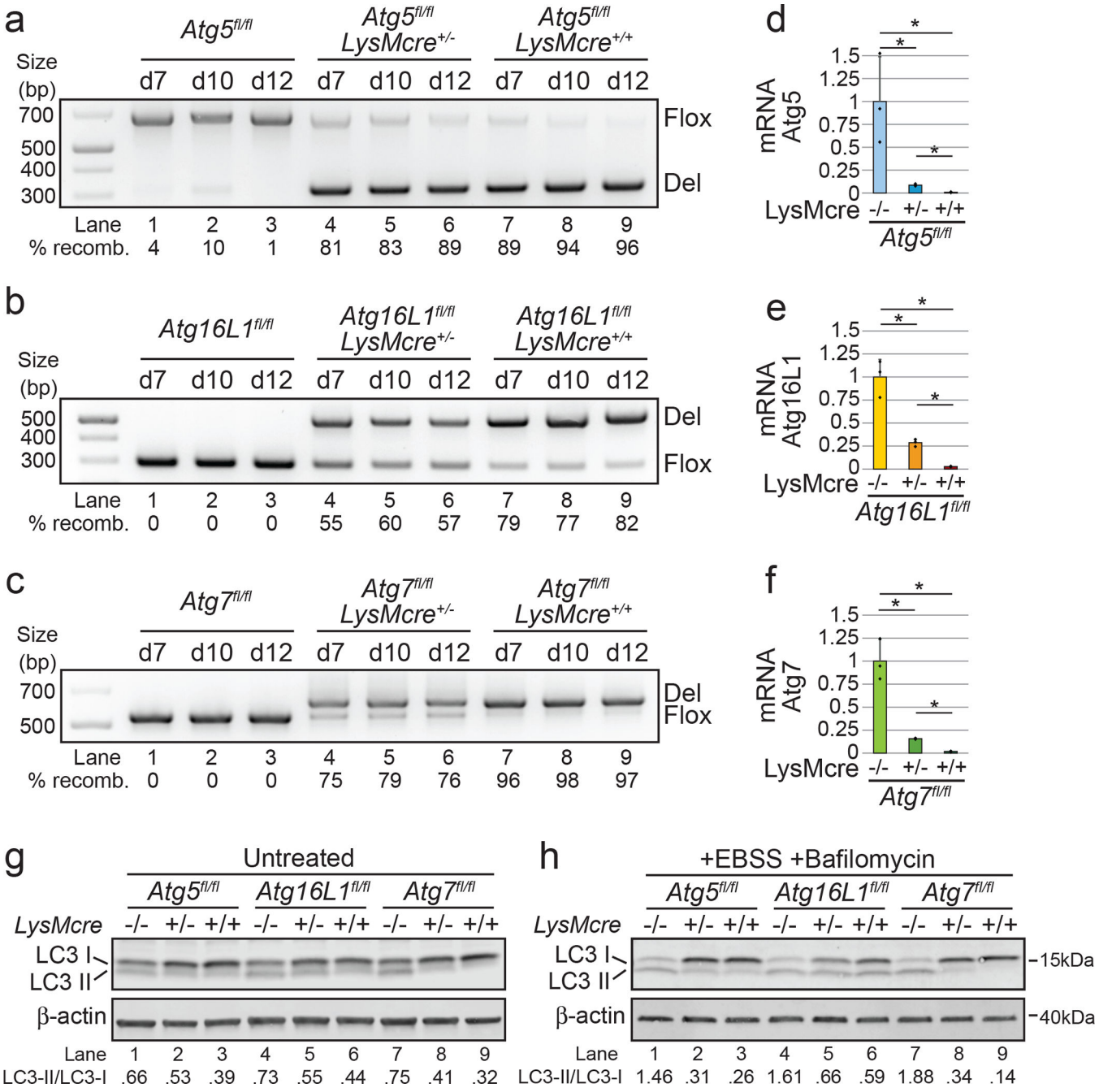

Fig. 1 |. Cre–Lox recombination efficiency in macrophages varies between different autophagy factors and is influenced by Cre dosage.

a–**c**, Analysis of Cre–Lox recombination efficiency in BMMs differentiated for 7, 10 or 12 days. Percentage of intensity of deleted band over combined intensities of floxed (Flox) and deleted (Del) bands is indicated by 'Percentage recombination'. **a**–**c**, Samples extracted from *Atg5*$^{fl/fl}$, *Atg5*$^{fl/fl}$ *LysMcre*$^{+/-}$ and *Atg5*$^{fl/fl}$ *LysMcre*$^{+/+}$ mice (**a**), *Atg16L1*$^{fl/fl}$, *Atg16L1*$^{fl/fl}$ *LysMcre*$^{+/-}$ and *Atg16L1*$^{fl/fl}$ *LysMcre*$^{+/+}$ mice (**b**) and *Atg7*$^{fl/fl}$, *Atg7*$^{fl/fl}$ *LysMcre*$^{+/-}$ and *Atg7*$^{fl/fl}$ *LysMcre*$^{+/+}$ mice (**c**). **d**–**f**, Measurement of mRNA levels of autophagy factors in BMMs differentiated for 10 days from *Atg5*$^{fl/fl}$, *Atg5*$^{fl/fl}$ *LysMcre*$^{+/-}$ and *Atg5*$^{fl/fl}$

LysMcre$^{+/+}$ mice (**d**), *Atg16L1*$^{fl/fl}$, *Atg16L1*$^{fl/fl}$ *LysMcre*$^{+/-}$ and *Atg16L1*$^{fl/fl}$ *LysMcre*$^{+/+}$ mice (**e**) and *Atg7*$^{fl/fl}$, *Atg7*$^{fl/fl}$ *LysMcre*$^{+/-}$ and *Atg7*$^{fl/fl}$ *LysMcre*$^{+/+}$ mice (**f**). Results are the means ± s.d. from three biological replicates. *$P \leq 0.05$ by two-sided *t*-test. **g**,**h**, Western blot analysis of LC3 and β-actin in BMMs differentiated for 12 days: samples are from untreated cells (**g**) or cells treated for 8 h with EBSS and 2 h with bafilomycin (**h**). Results are representative from two biological replicates.

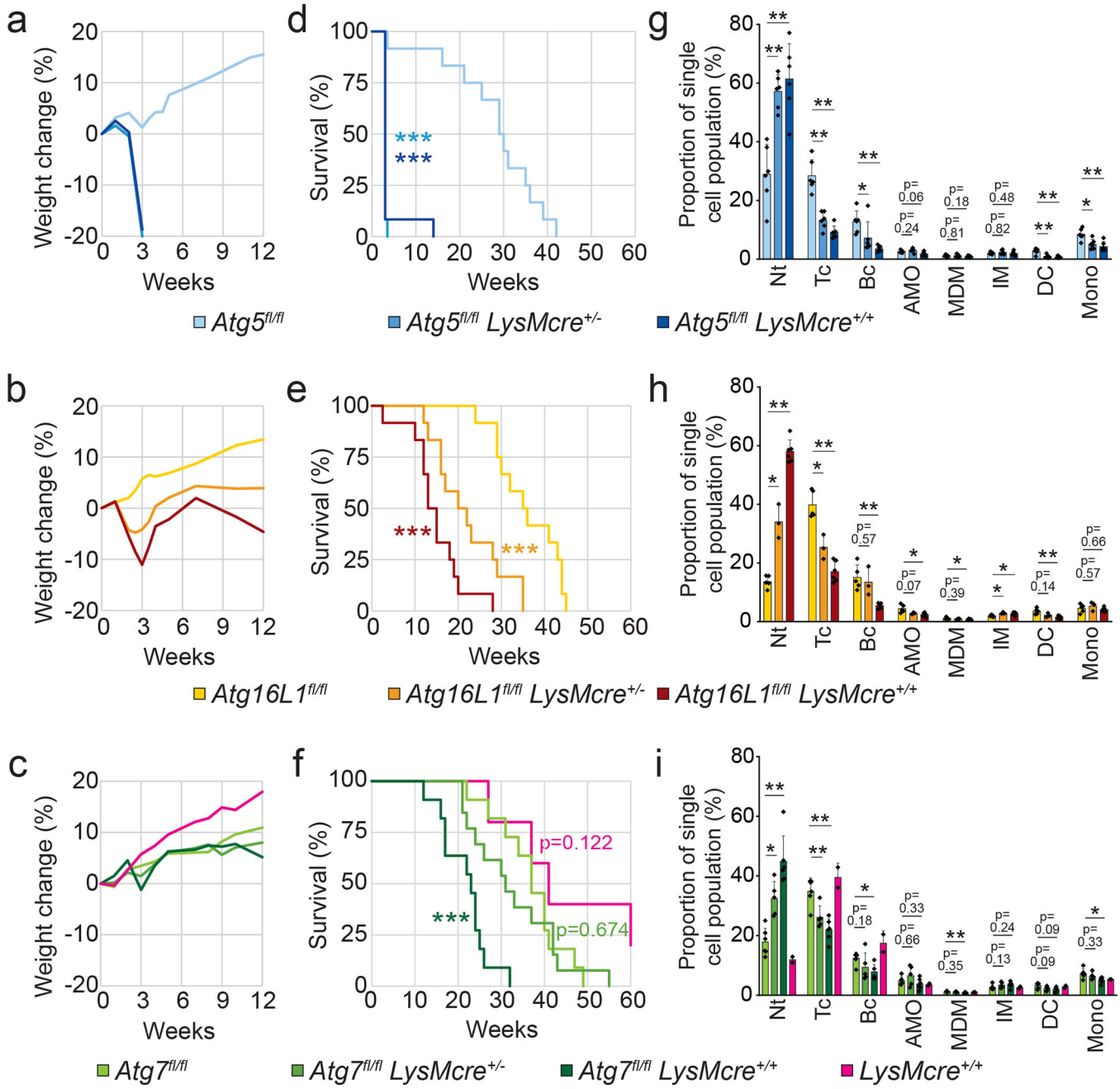

Fig. 2 |. *ATG16L1* and *ATG7* are required for control of *M. tuberculosis* at later stages of infection but the mouse phenotype is undermined by limitations of the Cre–Lox system.

a–**f**, Mice were infected with ~100 c.f.u. of *M. tuberculosis* and tracked for weight change (**a**–**c**) and survival (**d**–**f**). Each group was composed of 10–12 mice, except *LysMcre*$^{+/+}$ mice ($n = 5$). **a**–**c**, Weight change over the first 12 weeks of infection of *Atg5*$^{fl/fl}$, *Atg5*$^{fl/fl}$ *LysMcre*$^{+/-}$ and *Atg5*$^{fl/fl}$ *LysMcre*$^{+/+}$ mice (**a**), *Atg16L1*$^{fl/fl}$, *Atg16L1*$^{fl/fl}$ *LysMcre*$^{+/-}$ and *Atg16L1*$^{fl/fl}$ *LysMcre*$^{+/+}$ mice (**b**) and *Atg7*$^{fl/fl}$, *Atg7*$^{fl/fl}$ *LysMcre*$^{+/-}$, *Atg7*$^{fl/fl}$ *LysMcre*$^{+/+}$ and *LysMcre*$^{+/+}$ mice (**c**). **d**–**f**, Survival of *Atg5*$^{fl/fl}$, *Atg5*$^{fl/fl}$ *LysMcre*$^{+/-}$ and *Atg5*$^{fl/fl}$ *LysMcre*$^{+/+}$ mice (**d**), *Atg16L1*$^{fl/fl}$, *Atg16L1*$^{fl/fl}$ *LysMcre*$^{+/-}$ and *Atg16L1*$^{fl/fl}$ *LysMcre*$^{+/+}$

mice (**e**) and *Atg7*$^{fl/fl}$, *Atg7*$^{fl/fl}$ *LysMcre*$^{+/-}$, *Atg7*$^{fl/fl}$ *LysMcre*$^{+/+}$ and *LysMcre*$^{+/+}$ mice (**f**). Statistical significance was tested against the flox control group with a two-sided log-rank (Mantel–Cox) test. ***$P \leq 0.001$. **g**–**i**, Proportion of immune cell populations in the lungs of *Atg5* (**g**), *Atg16L1* (**h**) and *Atg7* (**i**) mutant mice infected for 21 days with *M. tuberculosis*. Results are the means ± s.d. from 2–7 mice per condition. Nt, neutrophils; Tc, T cells; Bc, B cells; AMO, alveolar macrophages; MDM, monocyte-derived macrophages; IM, interstitial macrophages; DC, dendritic cells; Mono, Ly6Chi inflammatory monocytes. For statistical analysis, *LysMcre*$^{+/-}$ and *LysMcre*$^{+/+}$ conditions were compared to the respective *LysM*$^{wt/wt}$ control. *$P \leq 0.05$, **$P \leq 0.01$, ***$P \leq 0.001$ by Mann–Whitney test.

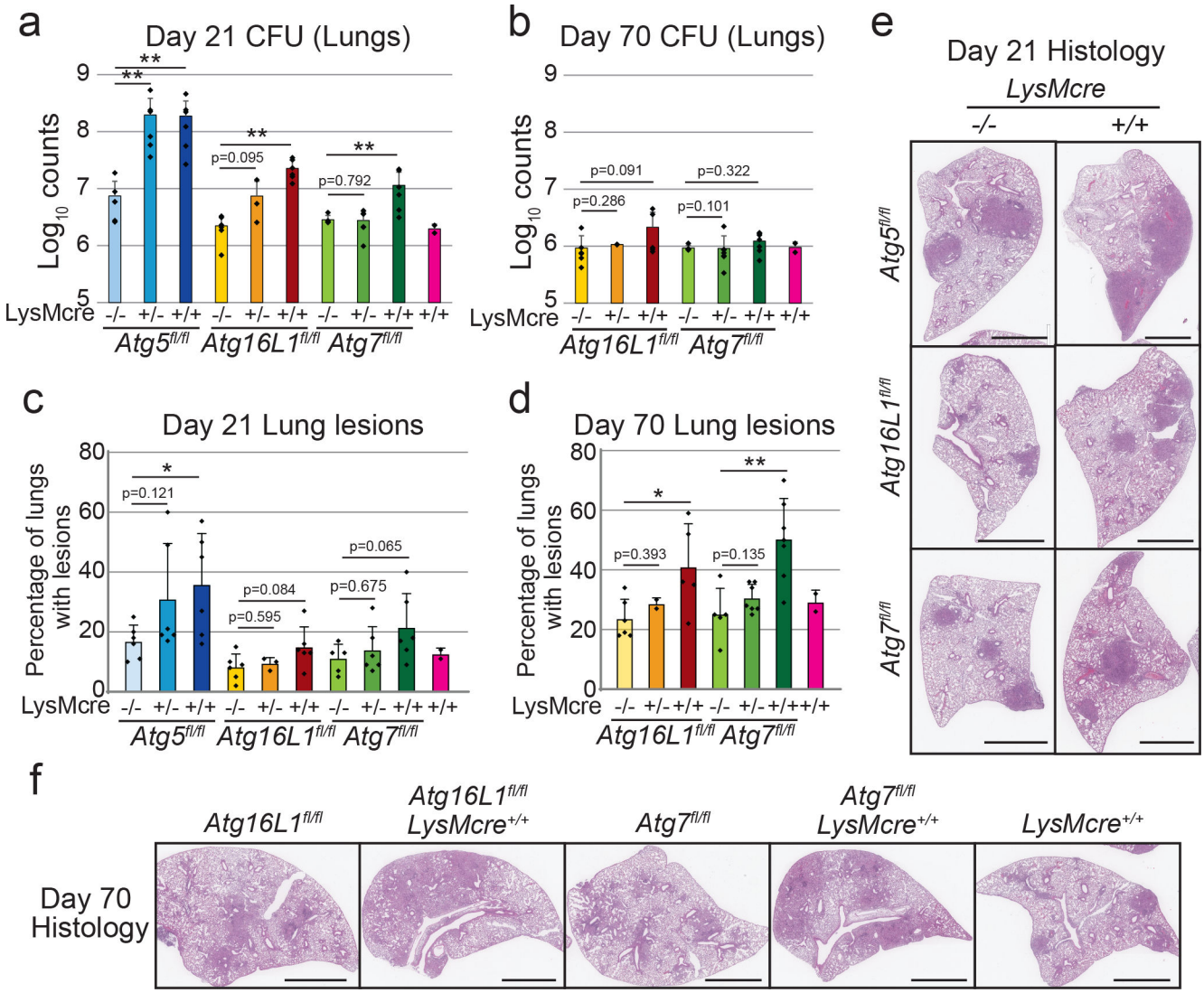

Fig. 3 |. *Atg16L1* and *Atg7* mutant mice display lung lesions at later stages of infection with *M. tuberculosis*.

a,**b**, The c.f.u. counts from the lungs of mice infected with ~100 c.f.u of *M. tuberculosis*. Lungs were collected at 21 days (**a**) or 70 days (**b**) postinfection. Results are the means ± s.d. from 2–6 mice per condition. **c**–**f**, Segments of the lungs from the same mice as in **a** and **b** were processed for histology: average portion of the lungs presenting lesions was measured with ImageScope at day 21 (**c**) and day 70 (**d**) postinfection; results are the means ± s.d. from 2–6 mice per condition. **e**,**f**, Representative sections at day 21 (**e**) and day 70 (**f**) postinfection are presented. Scale bar, 2 mm. For statistical analysis for c.f.u. and histology experiments, *LysMcre*$^{+/-}$ and *LysMcre*$^{+/+}$ conditions were compared to the respective *LysM*$^{wt/wt}$ control. *$P \leq 0.05$, **$P \leq 0.01$, ***$P \leq 0.001$ by Mann–Whitney test.

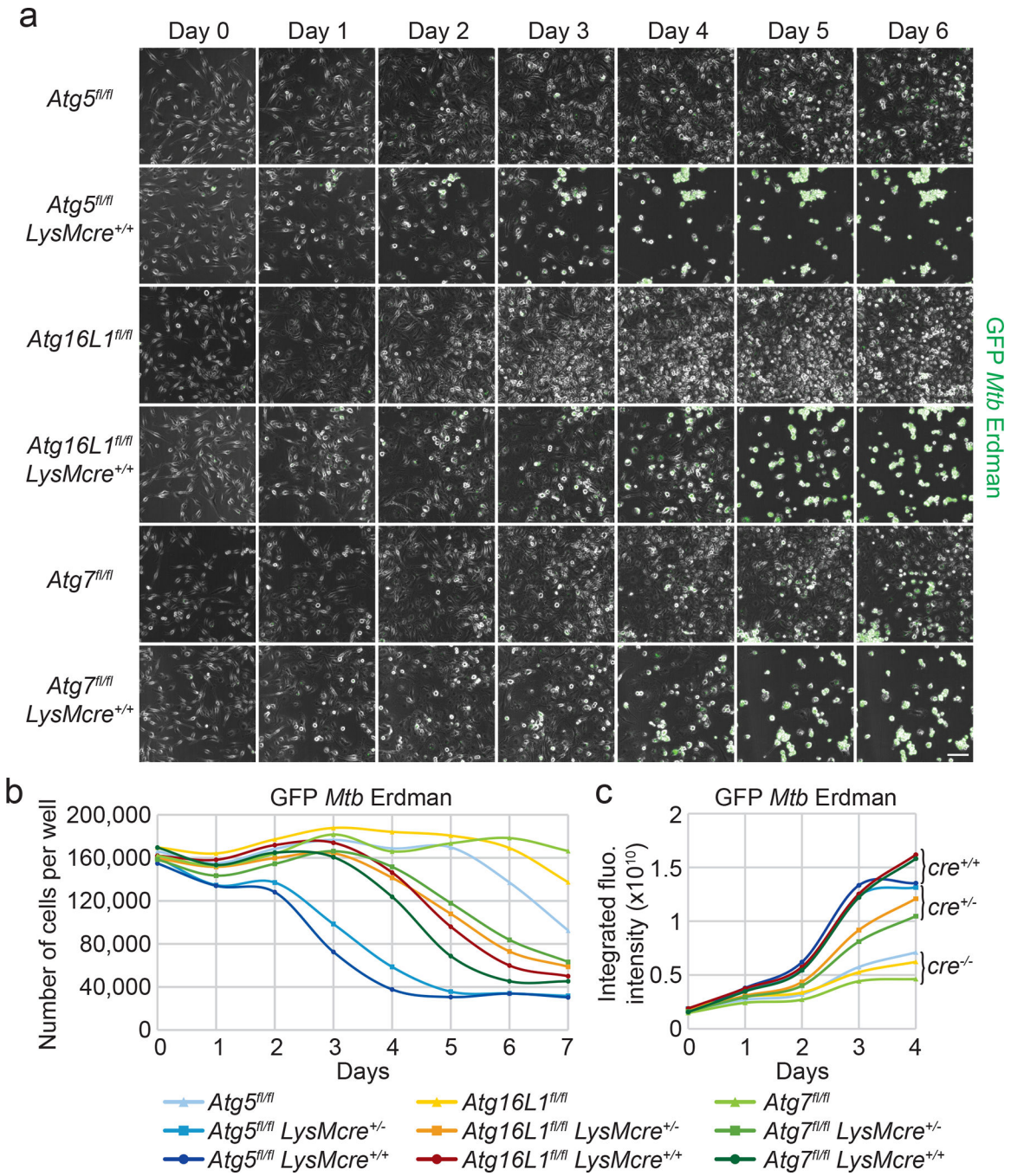

Fig. 4 |. Macrophages deficient in different autophagy factors are susceptible to *M. tuberculosis* infection.

a, Representative images from two independent experiments of a 6 days long time-lapse sequence of autophagy-deficient macrophages infected with GFP-expressing *M. tuberculosis* (*Mtb*) at an MOI of 2 (Supplementary Video 1). Scale bar, 100 μm. **b**,**c**, Macrophages infected with GFP-expressing *M. tuberculosis* at an MOI of 1 were imaged every day for 7 days by high-content microscopy. **b**,**c**, Number of cells (**b**) and integrated fluorescence intensity of GFP signal (**c**) were quantified over time. Data are the average of four technical

replicates from an experiment representative of two independent experiments. Statistics in Extended Data Fig. 4a,b.

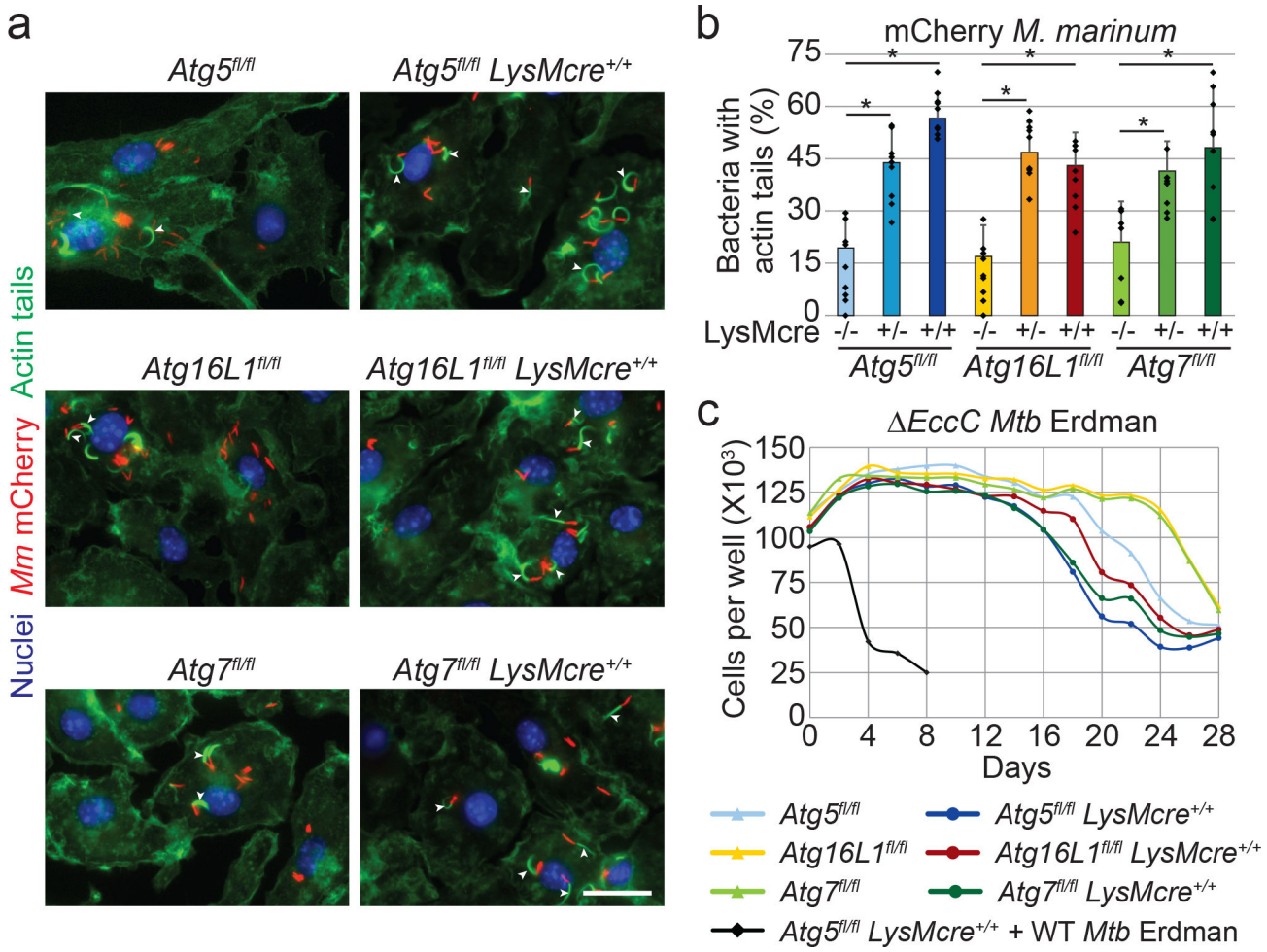

Fig. 5 |. The autophagy-deficient macrophage susceptibility to *M. tuberculosis* is ESX-1-dependent and linked to phagosome escape.

a, Illustrative images of actin tail formation by *M. marinum* (*Mm*) expressing mCherry inside macrophages at 11 h postinfection. Actin tails were stained with AlexaFluor 488 Phalloidin (green) and nuclei with dapi (blue). Arrowheads indicate examples of bacteria with actin tails. Scale bar, 20 μm. **b**, Quantification of the percentage of mCherry-expressing *M. marinum* colocalizing with actin tails after 11 h of infection of autophagy-deficient macrophages. Results are the means ± s.d. for ten images from two technical replicates. $*P \leq 0.05$ by two-sided *t*-test. **c**, Quantification of number of macrophages over time during time-course infection with GFP-expressing Δ*eccC M. tuberculosis* at an MOI of 1. Black curve shows survival of $Atg5^{fl/fl}$ $LysMcre^{+/+}$ macrophages infected with wild-type *M. tuberculosis*. Data are averaged from two independent experiments with each condition tested in technical duplicates. Statistics in Extended Data Fig. 7c.

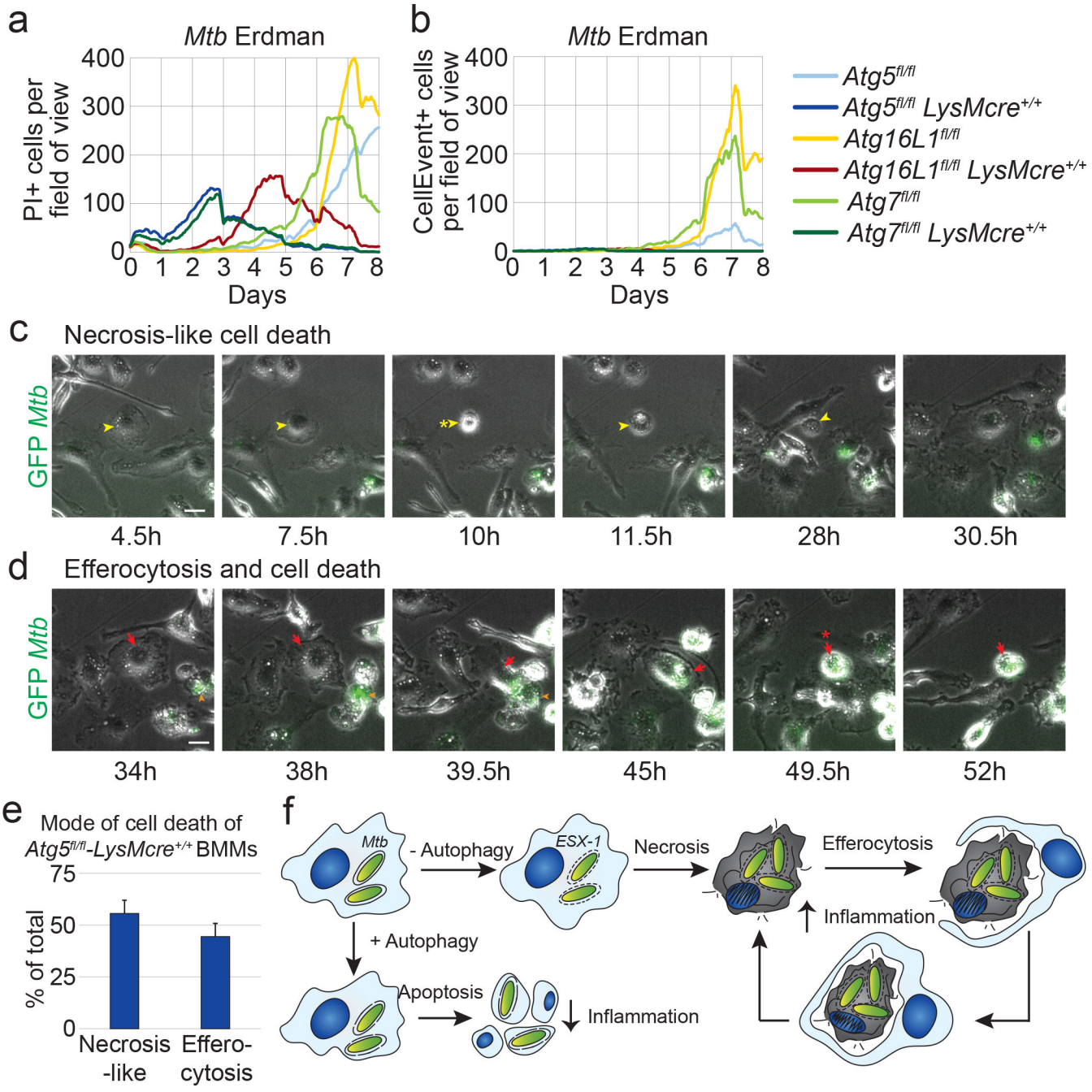

Fig. 6 |. *M. tuberculosis* infection induces necrosis-like cell death and efferocytosis in autophagy-deficient macrophages.

a,**b**, Autophagy-deficient macrophages were infected with *M. tuberculosis* at an MOI of 1. PI and CellEvent Caspase-3/7 reagent were added to the media at the beginning of the infection (Supplementary Video 2): number of PI-positive cells (**a**) and CellEvent-positive cells (**b**) per field of view was quantified over time. Results are the average of three technical replicates. Statistics are given in Extended Data Fig. 10b,c. **c**–**f**, *Atg5*$^{fl/fl}$ *LysMcre*$^{+/+}$ macrophages were infected with GFP-expressing *M. tuberculosis* and imaged every 30 min over a 6 day period (Supplementary Video 3). **c**, Illustrative images of necrosis-like cell

death. Yellow arrowhead shows dying cell, yellow asterisk denotes time of cell death. **d**, Illustrative images of efferocytosis followed by cell death. Macrophage (red arrow) dies (red asterisk) after phagocytosing an adjacent dead cell (orange arrowhead). **e**, Modes of cell death were recorded for 145 *Atg5*$^{fl/fl}$ *LysMcre*$^{+/+}$ macrophages infected with GFP-expressing *M. tuberculosis* from three independent experiments. The number of cells dying of necrosis-like cell death or after efferocytosis was quantified and presented as means ± s.d. (**c**). **f**, Model depicting that autophagy forestalls phagocyte cell death during infection and leads to non-inflammatory apoptosis. In the absence of autophagy, phagosome disruption mediated by bacterial ESX-1 induces rapid necrosis, followed by a cascade of efferocytosis and cell death that promotes inflammation.